Journal Pre-proofs


# Late Cretaceous adakitic and A-type granitoids in Chanang, southern Tibet: Implications for Neo-Tethyan slab rollback

Zhenzhen Wang, Zhidan Zhao, Xuping Li, Paul D. Asimow, Dong Liu, Xuanxue Mo, Ningyuan Qi, Yan Tang, Qing Wang, Di-Cheng Zhu, Liangliang Zhang, Lawangin Sheikh

PII: S1342-937X(21)00129-5
DOI: https://doi.org/10.1016/j.gr.2021.04.007
Reference: GR 2561

To appear in: *Gondwana Research*

Received Date: 16 January 2021
Revised Date: 9 April 2021
Accepted Date: 14 April 2021

Please cite this article as: Z. Wang, Z. Zhao, X. Li, P.D. Asimow, D. Liu, X. Mo, N. Qi, Y. Tang, Q. Wang, D-C. Zhu, L. Zhang, L. Sheikh, Late Cretaceous adakitic and A-type granitoids in Chanang, southern Tibet: Implications for Neo-Tethyan slab rollback, *Gondwana Research* (2021), doi: https://doi.org/10.1016/j.gr.2021.04.007

# Late Cretaceous adakitic and A-type granitoids in Chanang, southern Tibet: Implications for Neo-Tethyan slab rollback

Zhenzhen Wang[a,b], Zhidan Zhao[b,*], Xuping Li[a], Paul D. Asimow[c], Dong Liu[b], Xuanxue Mo[b], Ningyuan Qi[b], Yan Tang[b], Qing Wang[b], Di-Cheng Zhu[b], Liangliang Zhang[b], Lawangin Sheikh[d]

a. Research Center of Continental Dynamics, and College of Earth Science and Engineering, Shandong University of Science and Technology, Qingdao 266590, China

b. State Key Laboratory of Geological Processes and Mineral Resources, and School of Earth Science and Resources, China University of Geosciences, Beijing 100083, China

c. Division of Geological and Planetary Sciences, California Institute of Technology, Pasadena, CA 91125, USA

d. Department of Geology, University of Swabi, Anbar, KPK, Pakistan

**Manuscript submitted to Gondwana Research**

*Corresponding author at:

29 Xueyuan Road, Haidian District, Beijing 100083, China.

Fax: (+86-10) 8232-1115; Telephone: (+86) 1368-111-8299

E-mail: zdzhao@cugb.edu.cn

## Abstract

The co-existence of Cretaceous adakitic and A-type granitoids in southern Tibet can offer fundamental constraints on subduction of the Neo-Tethyan oceanic plate and associated crustal growth processes, if their petrogenetic relationships are understood. Here, we report whole-rock geochemistry, zircon U-Pb geochronology, *in situ* zircon Hf isotopes and zircon trace elements from the Chanang intrusive suite, including the Zeyu and Cuojielin plutons. The Cuojielin pluton is composed of A-type quartz syenites with high $K_2O+Na_2O$, $FeO^T$, and Zr contents and distinct negative Eu anomalies, consistent with fractional crystallization of mafic magma in a reducing, low-pressure, high-temperature environment. The adakitic Zeyu pluton, by contrast, has a strikingly high density of mafic enclaves. The elemental and isotopic signatures of the Zeyu mafic enclaves indicate a hybrid origin by mixing of magmas derived from the mantle wedge and from juvenile lower crust. The adakitic Zeyu host rocks, with low MgO, Cr, and Ni contents, show typical characteristics which originate from residual or fractionated amphibole of juvenile lower crust. The co-existence of aluminous A2-type granites and adakitic rocks indicates an anomalous high-temperature and relatively $H_2O$-rich environment. The synchronous regional occurrence of calc-alkaline magmatism, charnockites, granulite-facies metamorphism, back-arc extension, and generation of the two studied types of Chanang intrusive rocks can best be explained in the context of an episode of rollback of the Neo-Tethyan slab in the late Cretaceous.


**Key Words:** Adakitic rocks; A-type rocks; Slab rollback; Southern Tibet

## 1. Introduction

The widespread late Cretaceous magmatic rocks exposed in southern Tibet offer a unique view into geodynamic and geochemical interactions between the mantle and the crust in a subduction environment (Zhu et al., 2009; Meng et al., 2020; Zhang et al., 2020). However, the petrogenesis of these rocks was complex and, as a result, geodynamic models for their origin remain highly debated. Many such models have been proposed, including (i) steady northward subduction of the Neo-Tethyan oceanic plate (Jiang et al., 2012), (ii) subduction of a Neo-Tethyan mid-ocean ridge (Zheng et al., 2014), and (iii) episodic rollback of the trench and Neo-Tethyan slab (Ma et al., 2013, 2015). In some cases, different interpretations of particular individual plutonic suites, such as adakitic rocks, have led authors to adopt slab rollback or ridge subduction.

Slab rollback is generally driven by mantle flow pressure gradients or negative buoyancy anomalies (Nakakuki and Mura, 2013). With the down-going slab sinking vertically, the lithosphere commonly generates an upwelling of mantle wedge to compensate for the loss in volume in the mantle (Yin et al., 2017) and the overriding continental plate will passively follow the retreating trench, translating to extensional regime (Niu et al., 2014). The thermal anomaly caused by slab rollback will trigger the partial melting of asthenospheric mantle, oceanic slab, juvenile crustal materials, or thickened lower crust to produce the mafic rocks, I-type granite, A2-type granite, high-Mg or low-Mg adakitic magmas (Schlunegger and Kissling, 2015; Ji et al., 2019; Xu et al., 2019). The extension of the overriding plate generally induces the formation of bimodal igneous rocks and mafic dykes (Ma et al., 2015). In addition, the migration of igneous rocks towards ocean with ages decreasing along the path is a typical process of slab rollback (Jiang et al., 2018; Lipman et al., 1971). As for ridge subduction, it leads to the formation of a slab window, in which hot asthenospheric mantle wells up in the

gap created between the two diverging plates. There are several common geologic manifestations related to slab window migration, such as A-type rocks and adakitic rocks, OIB-type rocks in the volcanic arc, high temperature metamorphism (Brown, 1998; Groome et al., 2009; Li et al., 2012, 2016) and migration of igneous rocks further away from ocean (Sisson, 2003).

In the late Cretaceous of southern Tibet, granitoids with very different geochemical affinities co-exist in close proximity. Suites with adakitic affinities (high $SiO_2$, high Sr/Y, high La/Yb) can provide important insights into the mechanism of continental growth during the subduction of Neo-Tethyan oceanic plate (Ma et al., 2013; Xu et al., 2015; Zheng et al., 2014). On the other hand, A-type granitoids (high alkalis, high iron and high temperature) are generally attributed to extensional environments (Eby, 1992; Bonin, 2007) and so may attest to a change in the regional tectonic setting. Exploring the petrogenesis of both adakitic and A-type granitoids in the southern Lhasa terrane, and the temporal and genetic relationship between them, therefore offer the potential for valuable constraints on the tectonics and geodynamic of southern Tibet in the Late Cretaceous.

Numerous recent studies have focused on the ~90 Ma adakitic magmatism in southern Tibet, which have variously concluded that they were generated by partial melting of the subducted Neo-Tethyan oceanic slab or of thickened lower crust of the southern Lhasa Terrane (Ma et al., 2013; Wen et al., 2008; Zhang et al., 2010). The associated A-type granitoids, however, have rarely been sampled or studied. In this study, we present whole-rock analytical results and detailed studies of zircons (U-Pb geochronology, Hf isotopes, trace element abundances) from quartz syenites, granites and mafic microgranular enclaves (MMEs) in the Chanang area. Our goal is to characterize the petrogenesis of coexisting high-Sr/Y and A-type granitoids and any

genetic relationship between them. Together with previously published data, this study highlights the critical role of slab rollback in generating late Cretaceous granitoids in southern Tibet and provides a detailed spatio-temporal pattern of the rollback process.

## 2. Geological setting and samples description

The Lhasa terrane of southern Tibet is separated on the northern side from the Qiangtang terrane by the Banggong-Nujiang suture zone (Yin and Harrison, 2000), and on the southern side from the Indian Plate by the Indus-Yarlung Zangbo suture zone (Fig. 1a). The Lhasa terrane can be subdivided by the Shiquan River–Nam Tso mélange zone and Luobadui–Milashan fault into the northern, central, and southern Lhasa subterranes (Zhu et al., 2011) (Fig. 1b). Mesozoic-Cenozoic magmatism is widespread in the southern Lhasa terrane (Mo et al., 2007). In previous studies, five magmatic episodes preserving different stages of the evolution of southern Tibet have been recognized: 366-252 Ma (Geng, 2007; Wang et al., 2020), 220-145 Ma (Ji et al., 2009; Zhu et al., 2011; Shui et al., 2017; Wei et al., 2020), 120-66 Ma (Zhang et al., 2010; Ji et al., 2014; Xu et al., 2015; Ma et al., 2013), 68-40 Ma (Mo et al., 2007, 2008; Ji et al., 2014; Zhu et al., 2017), and 33-8 Ma (Hou et al., 2004; Chung et al., 2009; Wang et al., 2020a).The tectonic settings with different stages of magmatism can be seen Table 1. The late Cretaceous episode is represented along much of the strike of the Himalayan orogen by the Gangdese batholith and associated volcanic successions (Fig. 1c).The Chanang intrusive suite forms a band of granitoid plutons parallel to and adjacent to the Indus-Yarlung Zangbo suture zone, in the southern Lhasa terrane. Two plutons in the Chanang area were investigated in this study, the Cuojielin and Zeyu plutons. The Zeyu pluton intruded into the Jurassic volcanic strata of the Sangri group (Fig. 1d) and consists of quartz syenites, granites, and mafic microgranular enclaves (MMEs). Throughout this paper, when we discuss the “host rocks” of the Zeyu pluton, this refers

to the Zeyu quartz syenites and granites (i.e., the host of the MMEs), not to the country rock of the Sangri group. The smaller Cuojielin pluton intruded into both the Sangri group and the Zeyu pluton; it is mainly composed of quartz syenite.

The Cuojielin quartz syenite exhibits a fine-grained igneous texture and contains quartz (10-20% by volume), K-feldspar (60-65%), plagioclase (20-30%), amphibole (5-8%), biotite (5-10%) and minor accessory minerals (titanite, zircon, apatite, magnetite, etc.). The Zeyu quartz syenite is mainly composed of quartz (15-20%), K-feldspar (55-60%), plagioclase (25-30 %), biotite (5-8 %), amphibole (3-5%) and minor accessory minerals (titanite, apatite, magnetite, etc.). The Zeyu granite mainly consists of quartz (25-35 %), K-feldspar (55-60 %), plagioclase (15-25 %), and biotite (5-10%). MMEs are abundant in the Zeyu pluton. They may be spheroidal or deformed to elongated shapes. they show medium- to fine-grained igneous textures and are composed of quartz (2-5%), plagioclase (40-50 %), K-feldspar (45–50 %), amphibole (10-25 %), biotite (3-10 %), and needle-like apatite (Fig. 2).

## 3. Analytical methods

### 3.1 Zircon U-Pb isotopes, trace elements and Hf isotopes

Zircon grains were separated from the studied samples, mounted in epoxy resin, and polished to expose grain interiors. A Leo 1450VP scanning electron microscope at the Institute of Geology and Geophysics, Chinese Academy of Sciences (IGG-CAS), was used to obtain Cathodoluminescence (CL) images.

Laser ablation-inductively coupled plasma mass spectrometry (LA-ICPMS) was used for zircon U-Pb dating and trace element analyses at the State Key Laboratory of Geological Processes and Mineral Resources, China University of Geosciences at Wuhan (GPMR-CUG). The spot diameter was 32 μm. Zircon standard 91500 was used

as the external standard for U-Pb dating (Wiedenbeck et al., 1995). Details of the instrumental operating methods, off-line selection and integration of background and sample signals, time-dependent drift correction and quantitative calibration are summarized in Liu et al. (2010).

A Neptune multi-collector (MC)-ICPMS at the GPMR-CUG equipped with a 193-nm excimer laser-ablation system was used for Zircon Hf isotope ratio measurements. The spot diameter was 60 μm and its pulse frequency was 8 Hz. The average $^{176}Hf/^{177}Hf$ ratios for the Mud Tank and GJ-1 were 0.282489 ± 0.000005 (2SD, n = 36) and 0.282013 ± 0.000005 (2SD, n = 40), respectively, agreeing with the recommended values (Woodhead and Hergt, 2005). The detailed operating conditions for MC-ICPMS and interference correction method were described by Hu et al. (2012a and 2012b).

### 3.2 Major and trace elements

For whole-rock geochemical analysis, fresh samples were crushed to 200 mesh in a clean agate jaw crusher and powdered in an agate ball-mill. Loss on ignition was calculated by difference of sample weight between before and after heating by muffle furnace. Major elements were analyzed by direct-reading inductively coupled plasma emission spectrometer (ICP-AES) at China University of Geosciences at Beijing. The analytical precision of $SiO_2$, $TiO_2$, $Al_2O_3$, $Fe_2O_3$, CaO, MgO, $K_2O$, and $Na_2O$ is better than 3%, whereas the analytical precision of MnO and $P_2O_5$ is better than 5%. Whole-rock trace element abundances were determined with an *Agilent 7500a* ICP-MS at GPMR-CUG. 50 mg splits of sample powder were digested in a mixture of HF and $HNO_3$ by heating in Teflon bombs at 190 °C for 48 h. After evaporating to dryness at 115 ℃, dried samples were refluxed by using 30% $HNO_3$. The final solutions were diluted in polyethylene bottles to ~100 mL with 2% $HNO_3$. The detailed sample-preparation procedure and operating conditions have been described by Liu et al. (2008).

### 3.3 Whole-rock Sr-Nd isotopes

A Thermo-Finnigan TRITON thermal ionization mass spectrometer (TIMS) at the Institute of Geology and Mineral Resources, Tianjin, was used for whole-rock Sr and Nd isotope ratio measurements. Chemical separations were performed using conventional ion exchange procedures. Measured Sr and Nd isotope ratios were normalized against $^{86}Sr/^{88}Sr=0.1194$ and $^{146}Nd/^{144}Nd=0.7219$, respectively. Analytical results for Sr and Nd standards, reported by Liu et al. (2017), are in agreement with the recommended values (Liu et al., 2017). The detailed sample preparation procedure and operating conditions have been described by Zhang et al. (2002).

## 4. Results

### 4.1 Zircon geochronology and Hf isotopes

Zircon U-Pb dating results are provided in Table S2. Zircon grains from Zeyu samples are colorless and euhedral, with elongation ratios ranging from 1:1 to 2:1. These zircons display clear oscillatory zoning in CL images and have high Th/U (0.73 – 1.14) (Table S4). Sample SK1303 yielded a weighted mean $^{206}Pb/^{238}U$ age of 95.0 ± 0.5 Ma (MSWD = 0.8, fig. 3a). Sample SK1308 yielded a weighted mean $^{206}Pb/^{238}U$ age of 96.2 ± 0.6 Ma (MSWD = 1.1, fig. 3b). Sample SK1310 yielded a weighted mean $^{206}Pb/^{238}U$ age of 98.7 ± 1.0 Ma (MSWD = 1.4, fig. 3c).

Zircon grains from a Cuojielin quartz syenite are colorless and euhedral, with elongation ratios of 1:1 to 3:1. These grains have oscillatory CL zoning and variable concentrations of U (118 - 731 μg/g) and Th (81 - 784 μg/g). Sample SK1314 yielded a weighted mean $^{206}Pb/^{238}U$ age of 92.1 ± 1.1 Ma (MSWD = 1.3, fig. 3d).

Zircon Hf isotope data are provided in Table S3. Zircons from the Zeyu pluton have a wide range of Hf isotopic composition, with $^{176}Hf/^{177}Hf$ ranging from 0.282996

- 0.283144 and $\varepsilon_{Hf}(t)$ varying +9.9 between +15.0. According to the calculation of Mišković and Schaltegger (2009), the percentage mantle contribution to the Zeyu pluton could be as high as 94% (Fig. 6b).

### 4.2 Major and trace element geochemistry

The whole-rock major and trace element results are given in Table S1.

The host rocks of the Zeyu pluton have high $SiO_2$ (65.5 - 70.3 wt.%) and $K_2O$ (3.5 - 4.6 wt.%) contents but low MgO (0.7 - 1.4 wt.%), $Mg^{\#}$ (43.1 - 46.4), Cr (2.5 - 4.1 μg/g), and Ni (3.4 - 5.4 μg/g). They are high-K calc-alkaline, metaluminous rocks (A/CNK= 0.90 - 0.96) (Figs. 4a-c). The MMEs in the Zeyu pluton have much lower $SiO_2$ (53.5 - 54.8 wt.%) and $K_2O$ (1.6 – 2.0 wt.%) contents but high MgO (3.5- 3.6 wt.%), $Mg^{\#}$ (47.7- 49.6), Cr (7.0 - 26.2 μg/g), and Ni (10.6 - 18.9 μg/g). They are metaluminous (A/CNK= 0.66 - 0.72) and range from calk-alkaline to high-K calc-alkaline. On a chondrite-normalized rare earth element (REE) distribution diagram (Fig. 5a), all Zeyu host rocks are significantly enriched in light REEs (LREEs) relative to heavy REEs (HREEs) and exhibit negligible Eu anomalies (Eu/Eu* = 0.88 -1.07; $Eu/Eu^* \equiv (Eu)_N/\sqrt{(Gd)_N(Sm)_N}$). The REE patterns of MMEs are approximately parallel to those of host rocks but, surprisingly given their more primitive major element composition, are more enriched in REE. On a primitive mantle-normalized trace element distribution diagram (Fig. 5b), the Zeyu host rocks and MMEs show relative enrichment of large ion lithophile elements (LILEs) (e.g., Rb, Ba, Th, and U) and depletions of high field strength elements (HFSEs) (e.g., Nb, Ta, P, Ti).

The Cuojielin quartz syenites contain moderate $SiO_2$ (60.4 – 66.2 wt.%), low MgO (1.2 – 1.8 wt.%), and low compatible element (e.g., Cr and Ni; Table S1) concentrations, but high $K_2O$ (4.6 – 5.3 wt.%) and $Na_2O$ (3.9 – 4.2 wt.%) contents. Although metaluminous, they plot with the shoshonite series. The Cuojielin quartz syenites have

higher total REE contents than the Zeyu quartz syenites, with moderate LREE enrichment distinctly negative Eu anomalies (Eu/Eu* = 0.58 - 0.72) (Fig. 5c). On a primitive mantle-normalized trace element distribution diagram (Fig. 5d), the Cuojielin quartz syenites show slight depletions of some HFSEs (e.g., Nb, Ta, Ti) but enrichments Zr and Hf.

### 4.3 Whole rock Sr-Nd

Whole-rock Sr–Nd isotopic compositions are provided in Table S1.

The host rocks and MMEs in the Zeyu pluton all have relatively homogeneous Nd isotope ratios ($^{143}Nd/^{144}Nd_i$ = 0.512720 - 0.512736 and $\varepsilon_{Nd}(t)$ = +4.1 - +4.3; Table 1). The Cuojielin quartz syenites, similarly, have homogeneous Nd isotopic composition ($^{143}Nd/^{144}Nd_i$ = 0.512717 - 0.512732 and $\varepsilon_{Nd}(t)$ = +3.9 - +4.2; Table 1). As shown in Fig. 6a, the initial Sr-Nd isotopic compositions of Zeyu and Cuojielin intrusive rocks are comparable with those of the Jurassic volcanic rocks from the Yeba Formation.

### 4.4 Zircon trace elements

We studied trace elements in zircon in two quartz syenite samples, one from the Zeyu pluton (sample SK1310) and one from the Cuojielin pluton (sample SK1314). Their zircon trace elements concentrations, Ti-in-zircon crystallization temperatures, and oxygen fugacity calculated from trace elements are listed in Table S4.

Zircons in the quartz syenite of the Zeyu pluton are characterized by high total REEs (327-2206 μg/g), averaging 1074 μg/g. Their LREE/HREE ratios (0.03-0.05) indicate that they are all typical magmatic zircons. For zircons in sample SK1310, Ti contents are 4.1-10.7 μg/g, Hf contents are 6647-9765 μg/g and Eu/Eu* is 0.20-0.58 (average 0.26), showing obvious negative Eu anomalies. In the chondrite-normalized REE patterns, zircons in sample SK1310 show depletion of LREEs, enrichment of

HREEs, negative Eu anomaly and positive Ce anomaly (Fig. 7a).

The total REE content of zircons in quartz syenite (SK1314) in the Cuojielin pluton (sample SK1314) is high, 327-2206 μg/g (average 745 μg/g). LREE/HREE is 0.02-0.04, with an average of 0.03. The contents of Ti and Hf are 7.2-74.9 and 8523-11264 μg/g, respectively. Eu/Eu* is 0.15-0.46 (average 0.22). In the chondrite-normalized REE patterns, zircons in sample SK1314 show depletion of LREEs and enrichment of HREEs, as well as negative Eu anomaly and positive Ce anomaly (Fig. 7b). Trace elements of zircons can reflect the nature of magma source. Most zircons in samples SK1310 and SK1314 plot in the field of syenites in, e.g. Nb vs. Ta (Fig. 7c).

Studies have demonstrated that the incorporation of Ti into zircon depends on crystallization temperature, and that Ti concentration of zircon can therefore be used to estimate the magma crystallization temperature (Ferry and Watson, 2007). The calculated Ti-in-zircon temperatures of sample SK1310 are 639-725 ℃ (average 680 ℃) (Fig. 7d), and the calculated Ti-in-zircon temperatures of sample SK1314 are 684-933 ℃ (average 803 ℃). The Ce(IV)/Ce(III) ratio in zircons is sensitive to oxidation state during magma formation (Ballard et al., 2002) and so an estimate of the Ce(IV)/Ce(III) ratio in zircon based on the magnitude of the positive Ce anomaly constrains magmatic $fO_2$. Ce(IV)/Ce(III) ratios of zircons from sample SK1310 vary from 23-96 (average 48), whereas zircons in sample SK1314 have Ce(IV)/Ce(III) between 2.3 and 19 (average 6.7). It can be inferred that the Zeyu pluton formed in a low temperature and high oxygen fugacity environment, while the Cuojielin pluton formed in a relatively high temperature and reducing environment (Fig. 7d).

# 5. Discussion

## 5.1 Genetic types

Granites can be divided into M-type, I-type, S-type and A-type granites, a classification intended to separate them by the nature of their magma sources. M-type granites are considered to be mantle-derived, and show elevated contents of compatible elements, such as Cr and Ni (White, 1979). I-type granites are metaluminous, calc-alkaline, and typically show positive $\varepsilon_{Nd}(t)$, $\varepsilon_{Hf}(t)$ due to their derivation from partial melting of juvenile crust in island arc settings (Chappell and White, 1992). S-type granites are peraluminous, with high $Al_2O_3$ and enriched isotopic characteristics associated with melting of metasedimentary material in mature continental crust (Chappell and White, 1992). Finally, A-type granites are a diverse group rich in alkalies, iron and HFSEs (Bonin, 2007) that are associated with melting in low-water-activity, high-temperature, anorogenic settings such as extensional zones.

### *5.1.1 Zeyu Pluton: affinity to adakite*

The host quartz syenites, granites, and mafic microgranular enclaves of the Zeyu pluton are metaluminous and calc-alkaline with positive $\varepsilon_{Hf}(t)$ and $\varepsilon_{Nd}(t)$, low concentrations of Cr and Ni, and low Mg#. The $P_2O_5$ contents of felsic Zeyu samples in the Harker diagram decrease with increasing $SiO_2$ content, which is characteristic of I-type granites. Indeed, the Zeyu pluton is classified as I-type granite. The Zeyu host rocks, quartz syenites and granites have high $SiO_2$ ($\geqslant$56 wt.%), high Sr ($\geqslant$ 400 μg/g) and low Y ($\leqslant$ 18 μg/g) contents. In the defining discrimination diagrams for adakites (Defant and Drummond, 1990), all the Zeyu host rocks fall into the range of adakite (Figs. 8a-b).

*5.1.2 Cuojielin Pluton: A-type granitoid affinity*

Several lines of evidence presented in this study indicate that the Cuojielin quartz syenite pluton is an A-type granitoid; positive $\varepsilon_{Hf}(t)$ and $\varepsilon_{Nd}(t)$, low Cr and Ni contents, low Mg#, and metaluminous calc-alkaline affinity. S-type (peraluminous) and M-type (high Cr, Ni, and Mg#) affinities can be ruled out right away. The high concentrations of alkalies, iron and HFSEs, place the Cuojielin samples uniformly in A-type fields on I-S-A discrimination diagrams (Figs. 8c-d) (Whalen et al., 1987). Although the (10000 x Ga)/Al ratios of Cuojielin quartz syenite are lower than 2.6, the elevated alkali concentrations nevertheless place the samples in the A-type field in Fig. 8c. King et al. (1997) studied the A-type granites in the Lachlan fold belt of Australia and found that most of them had Zr contents greater than 301 μg/g, while those of evolved and primitive I-type granites averaged 151 μg/g and 116 μg/g Zr, respectively. The Zr contents in Cuojielin quartz syenites are all higher than 301 μg/g (average 373 μg/g), which is further evidence supporting the A-type classification. Moreover, the average value of (Zr + Nb + Ce + Y) in Cuojielin samples is 488 μg/g, which exceeds the lower limit (350 μg/g) for A-type granites (Fig. 8d) (King et al., 2001).

Since trace element concentrations are easily affected by crystallization and can push highly-evolved I-type granitoids into A-type fields, we check the affinity of the Cuojielin samples using the new method proposed by Frost et al. (2001) and Frost and Frost (2011), in $FeO^T/(FeO^T + MgO)$ and $(Na_2O+K_2O-CaO)$ vs. $SiO_2$ plots (Figs. 8e-f). The Cuojielin quartz syenites consistently fall into the area indicating A-type granite. The geochemistry of the Cuojielin pluton is similar to that of the A-type granite in the Banshiling area of South China (Li et al., 2012).

Lastly, previous studies have distinguished granite types by zircon saturation

temperature: S-types average 764 °C, I-types average 781 ℃ (King et al., 2001), and A-types range from 882 °C to 903 °C, with an average of 893 °C (Miller et al., 2003). Ti-in-zircon temperatures of zircons in Cuojielin samples (which should be lower than the zircon saturation temperature, as zircon continues to grow over a substantial temperature range of magmatic evolution) are mostly higher than 781 °C (Fig. 7d), with a maximum of 933 ℃ and an average of 803 ℃, consistent with the high-temperature origin of A-type granites.

To sum up, it can be concluded that the Cuojielin quartz syenite is an A-type granitoid.

**5.2 Petrogenesis**

*5.2.1 Evidence for magma mixing in generating MMEs in Zeyu pluton*

The abundance and ubiquity of mafic microgranular enclaves (MMEs) is striking in the Zeyu pluton (Figs. 2a and 2c). Several interpretations of MMEs in granitoids are offered in the literature: e.g., they may be remnants of incomplete binary mixing of felsic and mafic magmas (Feeley et al., 2008), cumulates from early in the crystallization sequence (Bonin, 2004), or restites left after partial melting of the source (Chen et al., 1989).

Noting the absence of either cumulate textures or inherited zircons in the Zeyu MMEs, we focus on testing the interpretation that MMEs in the Zeyu Pluton represent products of incomplete magma mixing. The following lines of evidence support this interpretation. First, most MMEs in the Zeyu Pluton exhibit elongate or spheroid shapes (Fig. 2a), consistent with plastic deformation in a partially crystallized convecting magma (Yang et al., 2015a). Second, we observe K-feldspar megacrysts that cross the boundaries between MMEs and their host rocks, which may indicate exchange of

crystals during magma mixing (Fig. 2a). Third, abundant acicular apatites in MMEs point to partial quenching of the MMEs as small volumes of hot mafic melt encountered cooler felsic magma (Vernon, 1984) (Fig. 2c). Fourth, in a number of variation diagrams, the Zeyu pluton host rock and MME samples cluster along opposite ends of a single linear trend (Figs. 4c-f), which is what would result if their compositional variations were the result of binary mixing. Finally, Zeyu MMEs and Zeyu host rocks show nearly parallel chondrite- and primitive mantle-normalized patterns, which may reflect the efficiency of elemental diffusion and homogenization in the liquid and partially molten states (Figs. 5a-b).

It is noteworthy that Zeyu MMEs show the typical trace-element pattern of island-arc igneous rocks, enriched in LILEs and slightly depleted in HFSEs (Fig. 5b). It is generally accepted that LILE enrichment in island-arc magmas is due to transfer of components from a subducted slab, through the mantle wedge, and into the upper plate arc crust. However, in detail subducted slabs contain multiple lithologies and each can contribute a distinctive geochemical signature to arc rocks by either melting or dehydrating. In diagrams aimed at separating the contributions of slab-derived melts from those of slab-derived fluids (Figs. 9a-b), the Zeyu MMEs generally lie closer to a fluid-addition trend.

The various samples of the Zeyu MMEs yield fairly homogeneous Sr-Nd isotope ratios. The range of $\varepsilon_{Nd}(t)$ and $^{87}Sr/^{86}Sr(i)$ values are +4.1-4.2 and 0.703220 -0.703371, respectively. Plotting $\varepsilon_{Nd}(t)$ vs. $^{87}Sr/^{86}Sr(i)$ (Fig. 6a), we see that the Zeyu MMES lie within the moderately depleted field defined by normal island arc magmatic rocks in the southern Lhasa terrane and overlap the field of early Jurassic volcanic rocks in the Yeba Formation. We conclude that the parental magma of the Zeyu MMEs likely originated from partial melting in the mantle wedge after metasomatism by subduction-

related fluids.

*5.2.2 Adakitic signature of Zeyu host rocks from residual or fractionated amphibole*

As described above, the host rocks, quartz syenites and granites of the Zeyu pluton show uniformly adakitic affinities. This signature, defined by high silica, Sr/Y and La/Yb, was originally proposed to be a unique diagnostic for partial melting of subducted oceanic crust with garnet-bearing residues (Defant and Drummond, 1990). However, alternative mechanisms for generating adakitic rocks have been proposed by subsequent studies, including (i) partial melting of garnet-bearing amphibolitic lower crust (Atherton and Petford, 1993); (ii) fractional crystallization of garnet and amphibole from mafic magmas (Macpherson et al., 2006), and (iii) magma mixing (Wang et al., 2020a). As illustrated in Fig. 10a, $^{87}Sr/^{86}Sr_i$ of Zeyu quartz syenites and granites decrease with the increase of $SiO_2$ contents, indicating that only a minor crustal component, but considerable mantle-derived melts (e.g., magma resembling MMEs), were involved in the evolution of Zeyu host rocks. Here we present geochemical evidences supporting that the adakitic signature of Zeyu host rocks, quartz syenites and granites, originate from residual or fractionated amphibole.

The Zeyu quartz syenites and granites are characterized by low MgO, Cr, and Ni contents and low $Mg^{\#}$ (< 42.5). Due to reaction with mantle wedge peridotite along the path from slab to arc, adakitic rocks derived from melts of delaminated lower crust or subducted oceanic crust usually have $Mg^{\#}$> 47 (Rapp et al., 1999). Low MgO contents (Fig. 4d), low $Mg^{\#}$ and low compatible element contents of the Zeyu quartz syenites and granites strongly argue against the possibility that the magma migrated through peridotite, a corollary of an origin from delaminated lower crust or subducted oceanic

crust (Wang et al., 2004). Second, compared with the Miocene adakitic rocks formed by partial melting of the thickened crust in Lhasa terrane, the Zeyu quartz syenites and granites have relatively lower $K_2O$ content and higher $\varepsilon_{Nd}(t)$ (Figs. 4c and 6a), indicating that the Zeyu quartz syenites and granites are derived from juvenile crust with few involvements of enriched mantle and/or upper crust components, similar to late Cretaceous adakitic rocks. In the discrimination diagrams of magma source, Zeyu quartz syenites and granites are consistent with the trend of 7%-Grt amphibolite, while more Miocene adakitic rocks corroborate the eclogite or 30%-Grt amphibolite trend (Fig 8b). Experimental determinations of partition coefficients appropriate for hydrous, felsic melts have consistently shown garnet is very strongly enriched in HREEs, whereas amphibole more effectively concentrates middle rare earth elements (MREEs) (Davidson et al., 2007). Thus, either varying degrees of partial melting with residual garnet or varying degrees of fractional crystallization of garnet would create positive correlation between $(La/Sm)_N$ and $(Dy/Yb)_N$ of melts. By contrast, residual or fractionated amphibole leads to increasing $(La/Sm)_N$ while $(Dy/Yb)_N$ decreases or remains constant. The Zeyu quartz syenites and granites show that $(Dy/Yb)_N$ decreases with increasing $(La/Sm)_N$ (Fig. 10b), an amphibole signature. The chondrite-normalized REE patterns for Zeyu quartz syenites and granites are visibly U-shaped (Fig. 5a), with minima in the MREEs, consistent with the influence of amphibole and not garnet. The La/Sm vs Sm/Yb discrimination diagram again indicates pyroxene and amphibole-bearing residue, and the absence of garnet (Fig. 10c).

Because La is more incompatible than Yb during partial melting (especially with residual amphibole or garnet), the correlation between La/Yb and La is thought to be able to distinguish between partial melting and fractional crystallization processes (Allègre and Minster, 1978). As illustrated in Fig. 10d, in the adakitic Zeyu quartz

syenites, La/Yb ratios are positively correlated with La contents, suggesting that the REE patterns preserve a signature of progressive partial melting and are not simply related to one another by fractional crystallization from a single primitive parent. Therefore, we infer that the Zeyu adakitic quartz syenites were formed by partial melting of juvenile lower crust enriched in amphibole. It is noteworthy that La/Yb ratios are relatively constant in Zeyu granites. This trend may suggest that fractional crystallization played an important role in the evolution of Zeyu granites (Fig. 10d). Associated with higher La/Sm ratios and Eu/Eu* in Zeyu granites than those in Zeyu quartz syenites (Figs. 10c, e), we propose that extensive fractionation of amphibole, rather than plagioclase, has taken place during the magma evolution of Zeyu granites, causing higher $SiO_2$ contents and Sr/Y ratios than Zeyu quartz syenites. Furthermore, constant $CaO/Na_2O$ ratios and variable $Al_2O_3/TiO_2$ can be seen in Fig.10f, reflecting negligible fractionation of plagioclase but obvious fractionation of biotite in Zeyu granites (Sylvester, 1998).

To sum up, the adakitic signature of Zeyu quartz syenites are induced by the partial melting of juvenile lower crust with amphibole as major residual phase, and the adakitic signature of Zeyu granites was then enhanced by further fractionation of amphibole and biotite.

*5.2.3 Fractional crystallization of Cuojielin pluton*

A range of genetic models for A-type granitoids with metaluminous or weakly peraluminous nature (King et al., 1997) have been proposed: (1) residual granitic melts produced by differentiation of originally alkaline mantle-derived magmas (Eby, 1992); (2) low-degree partial melts or products of extensive fractional crystallization of tholeiitic basalts (Frost and Frost, 2011); (3) anatexis of F-rich lower crustal granulites

(Whalen et al., 1987) or intermediate igneous rocks (tonalite and granodiorite) (Creaser et al., 1991) driven by heat supplied from underplating of mantle magma (Frost and Frost, 1997); and (4) hybrid origins with magmatic contributions from both mantle and crust (Yang et al., 2006).

The low compatible element concentrations and low $Mg^{\#}$ in the Cuojielin quartz syenites indicate that they are derived from an evolved source and are not primary products of mantle melting (Baker et al., 1995; Litvinovsky et al., 2015). However, as pointed out by Litvinovsky et al. (2015), peralkaline granites and syenites with high $K_2O$ and $Na_2O$ contents may in fact be derived from fractionation or originally mantle derived K-rich basaltic or andesitic magma, with little crustal contribution.

The four analyzed samples of Cuojielin quartz syenites cover a very small range in trace element composition, but shows increasing La at constant La/Yb, which is most consistent with the two more evolved Cuojielin samples (~66 wt.% $SiO_2$) being derived from the two more primitive Cuojielin samples (~61 wt.% $SiO_2$) mainly by fractional crystallization rather than distinct degrees of partial melting. However, it is difficult, given the evolved composition of the Cuojielin pluton and the absence of MMEs, to trace the fractionation back further to a uniquely constrained mantle-derived K-rich basaltic or andesitic magma. Nevertheless, we can infer from features that all the Cuojielin samples share (low Cr and Ni contents, high Rb/Sr ratios, distinctly negative Eu anomalies in the REE patterns, and negative P and Ti anomalies in the trace element patterns) that before emplacement the magma experienced fractionation of olivine, biotite, plagioclase, apatite, and a Ti-rich phase such as ilmenite. On the other hand, within the range of evolution captured by the available samples, Harker diagrams (Fig. 4) show decreases in $FeO^T$, MgO, CaO, $TiO_2$, and $P_2O_5$ contents with increasing $SiO_2$ content, suggesting continuing fractionation of pyroxene or amphibole, ilmenite or

titanite, and apatite.

Here, we construct a model to test whether the Zeyu MMEs (e.g., sample SK1306) might represent a primitive K-rich magma that could have evolved by fractional crystallization to form the Cuojielin quartz syenite compositions (Fig. 11). We assume a fractionating phase assemblage of 0.5 plagioclase, 0.15 clinopyroxene, 0.1 orthopyroxene, 0.1 biotite and 0.15 other accessory minerals. Key trace element features of the Cuojielin samples, including Rb/Sr ratio, Eu anomaly, level of REE enrichment, and LREE/HREE slope, can be reproduced by 30-60% fractional crystallization starting with a magma resembling the Zeyu MMEs. The development of negative Eu anomalies by plagioclase fractionation requires relatively reducing conditions for the proposed fractionation process.

### 5.3 Geodynamic implications

The southern Lhasa terrane experienced a magmatic peak in the late Cretaceous (100-80 Ma) during which a large volume of island arc magmatic rocks was emplaced, including gabbro, diabase, diorite and granite (Ji et al., 2009; Meng et al., 2019, 2020; Tang et al., 2019). The early portion of the flare-up period was dominated by basic and intermediate magma with a limited range of isotopic compositions, but the period from 95-90 Ma is marked by a wide range of $SiO_2$ contents (from ultramafic cumulates to high-$SiO_2$ granites) and extremely diverse isotopic compositions (Fig. 12a-b). A variety of unusual rocks with special properties — including high-Sr/Y adakitic rocks, upper crustal gabbros, A-type granites, and charnockites — were emplaced simultaneously in this period in the southern Lhasa terrane, indicating an unusual geodynamic environment.

Authors have suggested that the late Cretaceous (100 - 80 Ma) record in the southern Lhasa terrane preserves evidence of either (i) normal northward subduction of

the Neo-Tethyan oceanic slab (Jiang et al., 2012), (ii) an episode of mid-ocean ridge subduction (Zhang et al., 2010), or (iii) a period of rapid rollback of the trench and Neo-Tethyan oceanic plate (Meng et al., 2019). Here we consider these models in light of our results from the Chanang area.

Adakitic magmas are widespread in the late Cretaceous, along an extensive belt parallel to the Indus Yarlung-Zangbo Suture Zone. Ongoing normal subduction throughout the late Cretaceous does not explain the development of adakites. Moreover, oblique subduction of a mid-ocean ridge would likely affect only a local area of the southernmost Lhasa terrane at a given time, possibly producing local source of adakitic rocks, whereas the adakite belt extends all along the strike of the orogen with no obvious trend of age vs. longitude. Based on several lines of evidence discussed below, we suggest that the rollback of the Neo-Tethyan oceanic plate is the most reasonable geodynamic mechanism for southern Lhasa terrane in the late Cretaceous.

First, slab rollback causes major thermal anomalies more or less simultaneously along the strike of a subduction zone. The accelerated downwards motion of the subducted plate draws additional hot asthenospheric material upwards and into the mantle wedge, causing accelerated partial melting and underplating of the upper plate crust. Melting of the juvenile lower crust is followed by mixing between mantle- and crustally-derived melts at mid-crustal depths. The Zeyu pluton preserves evidence consistent with this series of processes: Zeyu MME's representing K-rich mantle-derived melts and adakitic Zeyu host rocks representing partial melts of juvenile lower crust were mixed to from the composite Zeyu pluton. A few million years later, the Cuojielin A-type granite was formed in a relatively high temperature environment. The average Ti-in-zircon temperature (802 ℃) and the average zircon saturation temperature (893 ℃) are both much higher than those in middle and upper-crustal

granites formed in normal arc settings (Ti-in-zircon temperatures average 781 ℃ in I-type granites and 764 °C in S-type granites). This is evidence that the severe thermal disturbance reached upper crustal levels in the southern Lhasa terrane by around 90 Ma. A variety of other rocks characteristic of a strongly elevated crustal geotherm at this time, including HT charnockitic magmatism and HT granulite faces metamorphism (Wang et al. 2009; Zhang et al., 2010; Ma et al., 2013) are found all along the strike of the southern Lhasa terrane and have likewise been attributed to the thermal anomaly induced by an episode of slab rollback and induced upwelling of asthenosphere.。 Moreover, ridge subduction would produce a high-temperature and relatively $H_2O$-poor magmas above the slab window (Xu et al., 2015), which is inconsistent with requirement of the residual or fractionated amphibole of Zeyu host rocks, as well as the existence of amphibole bearing A2-type rocks.

Second, slab rollback can give rise to back-arc extension (Heuret and Lallemand, 2005). In most cases, A-type granites are associated with extensional tectonic settings. Eby (1992) divided A-type granites into A1 and A2 subgroups. A1-type granites are associated with continental rifts or intraplate environments, which generally exist in ridge subduction setting and absent from slab rollback scenario. A2-type granites mainly derive from post-orogenic periods of continental collision zones or continental arc settings. The Cuojielin quartz syenites plot with A2-type granites, indicating a subduction-related extensional environment. The abundant late Cretaceous basic dikes throughout the southern Lhasa terrane have also been interpreted as evidence of a period of back-arc extension behind the Gangdese arc in the late Cretaceous (Tang et al., 2019). According to van Hinsbergen et al. (2011), changes in the trench position and dip angle of the subducting Neo-Tethyan slab correlate with globally significant plate tectonic events; the episode of rollback in the late Cretaceous likely drove sudden increase in

the convergence rate across the India-Asia collision at about 90 Ma.

Third, slab rollback and retreat of the volcanic front explains the migration of magmatic activity from north to south across the southern Lhasa terrane. Previous studies have shown a similar pattern at larger geographic and temporal scale: Late Jurassic and Early Cretaceous magmatic rocks are widely distributed in the central and northern terranes of the Lhasa block, while Late Cretaceous magmatic rocks are widely distributed only in the southern Lhasa terrane (Zhu et al., 2013). We tested for correlation between the ages and latitudes of dated late Cretaceous magmatic rocks using Pearson correlation analysis after deleting outliers with Mahalanobis distance >11 (Table S5). There is significant positive correlation between latitude and age (a 2-tailed significance test yields $p<0.01$), suggesting that along the whole magmatic front, over 500 km east-to-west, there is an apparent migration of late Cretaceous magmatic activity from north to south (Fig. 12c). Above all, we conclude that Neo-Tethyan slab rollback in late Cretaceous are responsible for the production of adakitic rocks, A2-type rocks and tectonic extension, as well as the oceanwards-receding of magmatic rocks.

## Conclusions:

(1) Geochronological data from the Chanang area indicate that the adakitic Zeyu pluton was emplaced in the late Cretaceous at 99-95 Ma and later intruded by the A-type Cuojielin quartz syenite at 92 Ma.

(2) The Zeyu adakitic quartz syenites were formed by partial melting of juvenile crust enriched in amphibole, and Zeyu adakitic granites originated from fractionation of amphibole and biotite. Zeyu adakitic magma mixed with a mantle-derived alkaline mafic magma preserved in part by the mafic enclaves (MMEs) found throughout the

Zeyu pluton. The Cuojielin A-type quartz syenites, on the other hand, could be generated as residual liquids after 30-60% fractional crystallization of a primitive magma with geochemical characteristics akin to those of the Zeyu MMEs.

(3) Lower crustal melting and ascent of K-rich mantle melts at ~95 Ma, followed by emplacement of high-temperature A-type granitoids at 92 Ma, along with the widespread along-strike development of adakitic rocks, charnockites, high-temperature metamorphism, and gradual southward migration of the locus of magmatism across the southern Lhasa terrane are all consistent with an episode of rollback of the Neo-Tethyan subduction system around 95-90 Ma.

## Acknowledgements

We thank the editor for handling this manuscript and two anonymous reviewers for constructive comments. We are grateful to Youqing Wei, Mingchun Dong, Han Yan, Jiayi Liu and Jinbao Yang for assistance of fieldwork in Tibet and geochemical analyses. This research was supported by the Second Tibetan Plateau Scientific Expedition and Research (STEP) program (grant 2019QZKK0702), the National Key Research and Development Project of China (project 2016YFC0600304), the Natural Science Foundation of China (grant 41802058), the Fundamental Research Funds for the Central Universities (grants 2652018122 and QZ05201902), and the 111 Project of the Ministry of Science and Technology of China (projects BP0719021 and B18048). ZW acknowledges a fellowship from the China Scholarship Council (CSC No. 201806400019).

## References:

Allègre, C.J., Minster, J.F., 1978. Quantitative models of trace element behavior in magmatic processes. Earth Planet. Sci. Lett. 38, 1-25.

Atherton, M. P., Petford, N., 1993. Generation of sodium-rich magmas from newly underplated basaltic crust. Nature 362, 144-146.

Baker, M. B., Hirschmann, M. M., Ghiorso, M. S., Stolper, E. M., 1995. Compositions of near-solidus peridotite melts from experiments and thermodynamic calculations. Nature 375, 308-311.

Ballard, J. R., Palin, M. J., Campbell, I. H., 2002. Relative oxidation states of magmas inferred from Ce(IV)/Ce(III) in zircon: application to porphyry copper deposits of northern Chile. Contrib. Mineral. Petrol. 144, 347-364.

Belousova, E. A., Griffin, W. L., O'Reilly, S. Y., Fisher, N. I., 2002. Igneous zircon: trace element composition as an indicator of source rock type. Contrib. Mineral. Petrol. 143, 602-622.

Bonin, B., 2004. Do coeval mafic and felsic magmas in post-collisional to within-plate regimes necessarily imply two contrasting, mantle and crustal, sources? A review. Lithos 78, 1-24.

Bonin, B., 2007. A-type granites and related rocks: Evolution of a concept, problems and prospects. Lithos 97, 1-29.

Boynton, W. V., 1984, Cosmochemistry of the rare earth elements: meteorite studies. Rare Earth Elem. Geochem. 63-114.

Brown, M., 1998. Ridge–trench interactions and high-T–low-P metamorphism, with particular reference to the Cretaceous evolution of the Japanese Islands. Geo. Soc. London Special Pub. 138, 131-163.

Chappell, B. W., White, A. J. R., 1992. I- and S-type granites in the Lachlan Fold Belt. T. Roy. Soc. Edin-Earth 83, 1-26.

Chen, Y., Price, R. C., White, A. J. R., 1989. Inclusions in Three S-Type Granites from Southeastern Australia. J. Petrol. 30, 1181-1218.

Chen, L., Qin, K. Z., Li, G. M., Li, J. X., Xiao, B., Zhao, J. X., Fan, X., 2015a. Zircon U–Pb ages, geochemistry, and Sr–Nd–Pb–Hf isotopes of the Nuri intrusive rocks in the Gangdese area, southern Tibet: Constraints on timing, petrogenesis, and tectonic transformation. Lithos 212-215, 379-396.

Chen, Y., Yang, J., Xiong, F., Zhang, L., Lei, S., Chen, M., 2015b.Geochronology and Geochemistry of the Subduction-related Rocks with High Sr/Y Ratios in the Zedong Area: Implications for the Magmatism in Southern Lhasa Terrane during Late Cretaceous. Acta. Petrol. Sin. (English Edition) 89, 351-368. Doi: 10.1111/1755-6724.12435

Chu, M. F., Chung, S. L., O'Reilly, S. Y., Pearson, N. J., Lee, H. Y., 2011. India's hidden inputs to Tibetan orogeny revealed by Hf isotopes of Transhimalayan zircons and host rocks. Earth Planet. Sci. Lett. 307, 479-486

Chung, S., Chu, M., Ji, J., O'Reilly, S. Y., Pearson, N. J., Liu, D., Lee, T., Lo, C., 2009. The nature and timing of crustal thickening in Southern Tibet: Geochemical and zircon Hf isotopic constraints from postcollisional adakites. Tectonophysics 477,

36-48.

Creaser, R. A., Price, R. C., Wormald, R. J., 1991. A-type granites revisited: Assessment of a residual-source model. Geology 19, 163.

Dai, Z., Li, G., Ding, J., Huang, Y., Cao, H., 2018. Late Cretaceous Adakite in Nuri Area, Tibet: Products of Ridge Subduction. Earth Sci.- J. China Univ. Geosci. 2727-2741 (in Chinese with English abstract).

Davidson, J., Turner, S., Handley, H., MacPherson, C., Dosseto, A., 2007. Amphibole "sponge" in arc crust? Geology 35, 787.

Defant, M. J., Drummond, M. S., 1990. Derivation of some modern arc magmas by melting of young subducted lithosphere. Nature 347, 662.

Eby, G. N., 1992. Chemical subdivision of the A-type granitoids: Petrogenetic and tectonic implications. Geology 20, 641.

Feeley, T. C., Wilson, L. F., Underwood, S. J., 2008. Distribution and compositions of magmatic inclusions in the Mount Helen dome, Lassen Volcanic Center, California: Insights into magma chamber processes. Lithos 106, 173-189.

Ferry, J. M., Watson, E. B., 2007. New thermodynamic models and revised calibrations for the Ti-in-zircon and Zr-in-rutile thermometers. Contrib. Mineral. Petrol. 154, 429-437.

Frost, C., Frost, B., 1997. Reduced rapakivi-type granites: The tholeiite connection. Geology 25, 647.

Frost, R. B., Barnes, C. G., Collins, W. J., Arculus, R. J., Ellis, D. J., 2001. A Geochemical Classification for Granitic Rocks. J. Petrol. 42, 2033-2-48.

Frost, C. D., Frost, B. R., 2011. On Ferroan (A-type) Granitoids: their Compositional Variability and Modes of Origin. J. Petrol. 52, 39-53.

Gao J., Zeng, L., Guo, C., Li, Q., Wang, Y., 2017. Late Cretaceous tectonics and magmatism in Gangdese batholith, Southern Tibet: A record from the mafic-dioritic dike swarms within the Baidui Complex. Acta. Petrol. Sin. 33, 2412-2436 (in Chinese with English abstract).

Geng, Q., 2007.The Late-Paleozoic Volcanic Rocks in the Gangdise Zone in Tibet: Petrology, Geochemistry and Tectonic Implications. China Univ Geosci, Doctoral Dissertation.

Groome, W., Thorkelson, D., 2009. The three-dimensional signature of ridge subduction and slab window migration. Tectonophysics 464, 70-83.

Guo, Z., Wilson, M., Zhang, M., Cheng, Z., Zhang, L., 2013. Post-collisional, K-rich mafic magmatism in south Tibet: constraints on Indian slab-to-wedge transport processes and plateau uplift. Contrib. Mineral. Petrol. 165, 1311-1340.

Heuret, A., Lallemand, S., 2005. Plate motions, slab dynamics and back-arc deformation. Phys. Earth Planet In. 149, 31-51.

Hou, Z., Gao, Y., Qu, X., Rui, Z., Mo, X., 2004. Origin of adakitic intrusives generated during mid-Miocene east–west extension in southern Tibet. Earth Planet. Sci. Lett. 220, 139-155.

Hu, Z., Liu, Y., Gao, S., Liu, W., Zhang, W., Tong, X., Lin, L., Zong, K., Li, M., Chen, H., 2012a. Improved in situ Hf isotope ratio analysis of zircon using newly designed X skimmer cone and jet sample cone in combination with the addition of

nitrogen by laser ablation multiple collector ICP-MS. J. Anal. Atom. Spectrom. 27, 1391-1399.

Hu, Z., Liu, Y., Gao, S., Xiao, S., Zhao, L., Günther, D., Li, M., Zhang, W., Zong, K., 2012b. A "wire" signal smoothing device for laser ablation inductively coupled plasma mass spectrometry analysis. Spectrochim. Acta. B. 78, 50-57.

Hu, Y., Liu, J., Ling, M., Liu, Y., Ding, X., Liu, D., Sun, W., 2017. Constraints on the origin of adakites and porphyry Cu-Mo mineralization in Chongjiang, Southern Gangdese, the Tibetan Plateau. Lithos 292, 424-436.

Huang, W., Liang, H., Zhang, J., Chen, X., Zhang, L., 2020. Formation of the Cretaceous skarn Cu–Au deposits of the southern Gangdese belt, Tibet: case studies of the Kelu and Sangbujiala deposits. Ore. Geol. Rev. 122, 103481.

Ji, W., Wu, F., Chung, S., Li, J., Liu, C., 2009. Zircon U–Pb geochronology and Hf isotopic constraints on petrogenesis of the Gangdese batholith, southern Tibet. Chem. Geol. 262, 229-245.

Ji, W., Wu, F., Chung, S., Liu, C., 2014. The Gangdese magmatic constraints on a latest Cretaceous lithospheric delamination of the Lhasa terrane, southern Tibet. Lithos 210-211, 168-180.

Ji, W., Wu, F., Chung, S., Wang, X., Liu, C. Z., Li, Q., Liu, X., Liu, X., Wang, J., 2016. Eocene Neo-Tethyan slab breakoff constrained by 45 Ma oceanic island basalt–type magmatism in southern Tibet. Geology 44, 283-286.

Ji, Z., Meng, Q., Wan, C., Ge, W., Yang, H., Zhang, Y., Dong, Y., Jin, X., 2019. Early Cretaceous adakitic lavas and A-type rhyolites in the Songliao Basin, NE China:

Implications for the mechanism of lithospheric extension. Gondwana Res. 71, 28-48.

Jiang, Z., Wang, Q., Li, Z., Wyman, D. A., Tang, G., Jia, X., Yang, Y., 2012. Late Cretaceous (ca. 90Ma) adakitic intrusive rocks in the Kelu area, Gangdese Belt (southern Tibet): Slab melting and implications for Cu–Au mineralization. J. Asian Earth Sci. 53, 67-81.

Jiang, Z., Wang, Q., Wyman, D. A., Li, Z., Yang, J., Shi, X., Ma, L., Tang, G., Gou, G., Jia, X., Guo, H., 2014. Transition from oceanic to continental lithosphere subduction in southern Tibet: Evidence from the Late Cretaceous–Early Oligocene (~91–30Ma) intrusive rocks in the Chanang–Zedong area, southern Gangdese. Lithos 196-197, 213-231.

Jiang, Z., Wang, Q., Wyman, D. A., Shi, X., Yang, J., Ma, L., Gou, G., 2015. Zircon U-Pb geochronology and geochemistry of Late Cretaceous-early Eocene granodiorites in the southern Gangdese batholith of Tibet: petrogenesis and implications for geodynamics and Cu ± Au ± Mo mineralization. Int. Geol. Rev. 57, 373-392.

Jiang, J. S., Zheng, Y. Y., Gao, S. B., Zhang, Y. C., Huang, J., Liu, J.., Wu, S., 2018. The newly-discovered Late Cretaceous igneous rocks in the Nuocang district: Products of ancient crust melting trigged by Neo–Tethyan slab rollback in the western Gangdese. Lithos 308-309, 294-315.

Kay, S. M., and Mpodozis, C., 2001. Central Andean Ore Deposits Linked to Evolving Shallow Subduction Systems and Thickening Crust. Geol. Soc. Am. Today Bull.

11, 4-9.

King, P. L., White, A. J. R., Chappell, B. W., Allen, C. M., 1997. Characterization and Origin of Aluminous A-type Granites from the Lachlan Fold Belt, Southeastern Australia. J. Petrol., 371-391.

King, P. L., Chappell, B. W., Allen, C. M., White, A. J. R., 2001. Are A-type granites the high-temperature felsic granites? Evidence from fractionated granites of the Wangrah Suite. J. Geol. Soc. Australia 48, 501-514.

Li, J., Qin, K., Li, G., Xiao, B., Chen, L., Zhao, J., 2011. Post-collisional ore-bearing adakitic porphyries from Gangdese porphyry copper belt, southern Tibet: melting of thickened juvenile arc lower crust. Lithos 126, 265-277.

Li, H., Ling, M., Li, C., Zhang, H., Ding, X., Yang, X., Fan,W., Li, Y., Sun, W., 2012. A-type granite belts of two chemical subgroups in central eastern China: Indication of ridge subduction. Lithos 150, 26-36.

Li, S., Zhu, D., Wang, Q., Zhao, Z., Zhang, L., Liu, S., Chang, Q., Lu, Y., Dai, J., Zheng, Y., 2016. Slab-derived adakites and subslab asthenosphere-derived OIB-type rocks at 156±2 Ma from the north of Gerze, central Tibet: Records of the Bangong–Nujiang oceanic ridge subduction during the Late Jurassic. Lithos 262, 456-469.

Li, Y., Li, X., Wang, C., Wei, Y., Chen, X., He, J., Xu, M., Hou, Y., 2017. Miocene adakitic intrusions in the Zhongba terrane: implications for the origin and geochemical variations of post-collisional adakitic rocks in southern Tibet. Gondwana Res. 41, 65-76.

Lipman, P.W., Christiansen, R.L., Prostka, H.J., 1971. Evolving subduction zones in the western United States, as interpreted from igneous rocks. Science 148, 821–825.

Litvinovsky, B. A., Jahn, B. M., Eyal, M., 2015. Mantle-derived sources of syenites from the A-type igneous suites-New approach to the provenance of alkaline silicic magmas. Lithos 232, 242-265.

Liu, Y., Hu, Z., Gao, S., Günther, D., Xu, J., Gao, C., Chen, H., 2008. In situ analysis of major and trace elements of anhydrous minerals by LA-ICP-MS without applying an internal standard. Chem. Geol. 257, 34-43.

Liu, Y., Hu, Z., Zong, K., Gao, C., Shan, G., 2010. Reappraisement and refinement of zircon U-Pb isotope and trace element analyses by LA-ICP-MS. Chinese Sci. Bull. 55, 1535-1546.

Liu, D., Zhao, Z., DePaolo, D. J., Zhu, D., Meng, F., Shi, Q., Wang, Q., 2017. Potassic volcanic rocks and adakitic intrusions in southern Tibet: Insights into mantle-crust interaction and mass transfer from Indian plate. Lithos 268-271, 48-64.

Liu, J., Xie, C., Li, C., Fan, J., Hao, Y., 2019. Origins and tectonic implications of Late Cretaceous adakite and primitive high-Mg andesite in the Songdo area, southern Lhasa subterrane, Tibet. Gondwana. Res. 76.

Ma, L., Wang, Q., Wyman, D. A., Li, Z., Jiang, Z., Yang, J., Gou, G., Guo, H., 2013. Late Cretaceous (100–89Ma) magnesian charnockites with adakitic affinities in the Milin area, eastern Gangdese: Partial melting of subducted oceanic crust and implications for crustal growth in southern Tibet. Lithos 175-176, 315-332.

Ma, L., Wang, Q., Wyman, D.A., Jiang, Z., Yang, J., Li, Q., Gou, G., Guo, H., 2013a. Late Cretaceous crustal growth in the Gangdese area, southern Tibet: Petrological and Sr–Nd–Hf–O isotopic evidence from Zhengga diorite–gabbro. Chem. Geol. 349, 54-70.

Ma, L., Wang, Q., Li, Z. X., Wyman, D. A., Jiang, Z. Q., Yang, J. H., Gou, G. N., Guo, H. F., 2013b. Early Late Cretaceous (ca. 93Ma) norites and hornblendites in the Milin area, eastern Gangdese: Lithosphere–asthenosphere interaction during slab roll-back and an insight into early Late Cretaceous (ca. 100-80Ma) magmatic "flare-up" in southern Lhasa. Lithos 172-173, 17-30.

Ma, L., Wang, Q., Wyman, D. A., Jiang, Z., Wu, F., Li, X., Yang, J., Gou, G., Guo, H., 2015. Late Cretaceous back-arc extension and arc system evolution in the Gangdese area, southern Tibet: Geochronological, petrological, and Sr-Nd-Hf-O isotopic evidence from Dagze diabases. J. Geophys. Res- Sol. Ea. 120, 6159-6181.

Macpherson, C. G., Dreher, S. T., Thirlwall, M. F., 2006. Adakites without slab melting: High pressure differentiation of island arc magma, Mindanao, the Philippines. Earth Planet. Sci. Lett. 243, 581-593.

Maniar, P. D., and Piccoli, P. M., 1989. Tectonic discrimination of granitoids. Geol. Soc. Am. Bull. 101, 635-643.

Meng, Y., Xiong, F., Xu, Z., Ma, X., 2019. Petrogenesis of Late Cretaceous mafic enclaves and their host granites in the Nyemo region of southern Tibet: Implications for the tectonic-magmatic evolution of the Central Gangdese Belt. J. Asian Earth Sci. 176, 27-41.

Meng, Y., Santosh, M., Mao, G., Lin, P., Liu, J., Ren, P., 2020. New constraints on the tectono-magmatic evolution of the central Gangdese belt from Late Cretaceous magmatic suite in southern Tibet. Gondwana Res. 80, 123-141.

Middlemost, E. A. K., 1994. Naming materials in the magma/igneous rock system. Annu. Rev. Earth Planet. Sci. 37, 215-224.

Miller, C. F., Mcdowell, S. M., Mapes, R. W., 2003. Hot and cold granites? Implications of zircon saturation temperatures and preservation of inheritance. Geology 31, 529.

Mišković, A., Schaltegger, U., 2009. Crustal growth along a non-collisional cratonic margin: A Lu–Hf isotopic survey of the Eastern Cordilleran granitoids of Peru. Earth Planet. Sci. Lett. 279, 303-315.

Mo, X., Hou, Z., Niu, Y., Dong, G., Qu, X., Zhao, Z., Yang, Z., 2007. Mantle contributions to crustal thickening during continental collision: Evidence from Cenozoic igneous rocks in southern Tibet. Lithos 96, 225-242.

Mo, X., Niu, Y., Dong, G., Zhao, Z., Hou, Z., Zhou, S., Ke, S., 2008. Contribution of syncollisional felsic magmatism to continental crust growth: A case study of the Paleogene Linzizong volcanic Succession in southern Tibet. Chem. Geol. 250, 49-67.

Nakakuki, T., Mura, E.,2013. Dynamics of slab rollback and induced back-arc basin formation. Earth Planet. Sci. Lett. 361, 287-297

Niu, Y., 2014. Geological understanding of plate tectonics: Basic concepts, illustrations, examples and new perspectives. Earth Planet. Sci. Lett. 10, 23-46.

Peccerillo, A., 1992. Potassic and ultrapotassic rocks: Compositional characteristics, petrogenesis, and geologic significance. Episodes 15, 243-251.

Petford, N., Atherton, M., 1996. Na-rich Partial Melts from Newly Underplated Basaltic Crust: the Cordillera Blanca Batholith, Peru. J. Petrol. 37, 1491-1521.

Rapp, R. P., Shimizu, N., Norman, M. D., Applegate, G. S., 1999. Reaction between slab-derived melts and peridotite in the mantle wedge: experimental constraints at 3.8 GPa. Chem. Geol. 160, 335-356.

Schlunegger, F., Kissling, E. 2015. Slab rollback orogeny in the Alps and evolution of the Swiss Molasse basin. Nat. Commun. 6, 6.

Shi, H., Duan, Z., Li, G. Zhang, L., 2020. Geochemistry and Genesis of the Late Cretaceous Granodiorite in Nulin, Tibet. Sedimentary Geology and Tethyan Geology 40, 71-82 (in Chinese with English abstract).

Shui, X., He Z., Klemd, R., Zhang, Z., Lu, T., Yan, L., 2017. Early Jurassic adakitic rocks in the southern Lhasa sub-terrane, southern Tibet: petrogenesis and geodynamic implications. Geol. Mag. 155, 132-148.

Sisson, V.B., Poole, A.R., Harris, N.R., Cooper-Burner, H., Pavlis, T.L., Copeland, P., Donelick, R. A., McClelland, W.C., 2003. Geochemical and geochronologic constraints for genesis of a tonalite-trondhjemite suite and associated mafic intrusive rocks in the eastern Chugach Mountains, Alaska: A record of ridge-transform subduction. Geol. Soc. Am. Special Paper 371, 293-326.

Stern, C. R., and Kilian, R., 1996. Role of the subducted slab, mantle wedge and continental crust in the generation of adakites from the Andean Austral Volcanic

Zone. Contrib. Mineral. Petrol. 123, 263-281.

Sun, S. S., McDonough, W. F., 1989. Chemical and isotopic systematics of oceanic basalts: implications for mantle composition and processes. Geo. Soc. London Special Pub. 42, 313-345.

Sun, X., Lu, Y.J., McCuaig, T.C., Zheng, Y.Y., Chang, H.F., Guo, F., Xu, L.J., 2018. Miocene ultrapotassic, high-Mg dioritic, and adakite-like rocks from Zhunuo in Southern Tibet: Implications for mantle metasomatism and porphyry copper mineralization in collisional orogens. J. Petrol. 59 341-386.

Sylvester, P.J., 1998. Post-collisional strongly peraluminous granites. Lithos 45, 29-44.

Tafti, R., 1961. Metallogeny, geochronology and tectonic setting of the Gangdese belt, southern Tibet, China, Doctoral dissertation.

Tang, Y., Zhao, Z., Qi, N., Wang, Z., Liu, D., Luan, J., Zhu, D., 2019. Geochemistry and petrogenesis of Late Cretaceous Namling gabbro and dykes in Gangdese batholith, Tibet. Acta. Petrol. Sin. 035, 387-404 (in Chinese with English abstract).

Tian, S., Yang, Z., Hou, Z., Mo, X., Hu, W., Zhao, Y., Zhao, X., 2017. Subduction of the Indian lower crust beneath southern Tibet revealed by the post-collisional potassic and ultrapotassic rocks in SW Tibet. Gondwana Res. 41, 29-50.

Van Hinsbergen, D. J. J., Steinberger, B., Doubrovine, P. V., Gassmöller, R., 2011. Acceleration and deceleration of India-Asia convergence since the Cretaceous: Roles of mantle plumes and continental collision. J. Geophys. Res-Sol. Ea. 116, B06101.

Vernon, R. H., 1984. Microgranitoid enclaves in granites—globules of hybrid magma

quenched in a plutonic environment. Nature 309, 438-439.

Wang, Q., Xu, J., Zhao, Z., Bao, Z., Xu, W., Xiong, X., 2004. Cretaceous high-potassium intrusive rocks in the Yueshan-Hongzhen area of east China: Adakites in an extensional tectonic regime within a continent. Geochem. J. 38, 417-434.

Wang, J., Zhang, Z., Xin, D., Feng, L., Fei, Y., Wei, W., 2009. Discovery of Late Cretaceous garnet two-pyroxene granulite in the southern Lhasa terrane, Tibet and its tectonic significances. Acta. Petrol. Sin. 25, 1695-1706.

Wang, X., Lang, X., Tang, J., Deng, Y., He, Q., Xie, F., Li, L., Yin, Q., Li, Z., Yang, Z., Dong, S., Ding, F., Wang, Z., Huang, Y., 2020. Early Carboniferous Back-Arc Rifting-Related Magmatism in Southern Tibet: Implications for the History of the Lhasa Terrane Separation From Gondwana. Tectonics 39, 10.1029/2020TC006237.

Wang, Z., Zhao, Z., Asimow, P. D., Liu, D., Sheikh, L., 2020a. Shoshonitic enclaves in the high Sr/Y Nyemo pluton, southern Tibet: Implications for Oligocene magma mixing and the onset of extension of the southern Lhasa terrane. Lithos 362, 105490.

Wei, Y., Zhao, Z., Niu, Y., Zhu, D., Donald, J. D., Jing, T., Liu, D., Guan, Q., Lawangin, S., 2020.Geochemistry, detrital zircon geochronology and Hf isotope of the clastic rocks in southern Tibet: Implications for the Jurassic-Cretaceous tectonic evolution of the Lhasa terrane. Gondwana Res. 78, 41-57.

Wen, D., Chung, S., Song, B., Iizuka, Y., Yang, H., Ji, J., Liu, D., Gallet, S., 2008. Late Cretaceous Gangdese intrusions of adakitic geochemical characteristics, SE Tibet:

Petrogenesis and tectonic implications. Lithos 105, 1-11.

Wen, D. R., Liu, D., Chung, S. L., Chu, M. F., Ji, J., Zhang, Q., Song, B., Lee, T. Y., Yeh, M. W., Lo, C. H., 2008a. Zircon SHRIMP U–Pb ages of the Gangdese Batholith and implications for Neotethyan subduction in southern Tibet. Chem. Geol. 252, 191-201.

Whalen, J. B., Currie, K. L., Chappell, B. W., 1987. A-type granites: geochemical characteristics, discrimination and petrogenesis. Contrib. Mineral. Petrol. 95, 407-419.

White, A. J. R., 1979. Source of granite magmas. Geol. Soc. Am. Memoir 159, 21-34.

Wiedenbeck, M., Allé, P., Corfu, F., Griffin, W. L., Meier, M., Oberli, F., Quadt, A. V., Roddick, J. C. and Spiegel, W., 1995. Three natural zircon standards for U-Th-Pb, Lu-Hf, trace element and REE analyses. Geostandards Newsletter 19, 1-23.

Woodhead, J., Hergt, J., 2005. A preliminary appraisal of seven natural zircon reference materials for in situ Hf isotope determination. Geostand. Geoanal. Res. 29,183-195.

Wu, C., Zheng, Y., Xu, B., Hou, Z., 2018. The genetic relationship between JTA–like magmas and typical adakites: An example from the Late Cretaceous Nuri complex, southern Tibet. Lithos 320-321, 265-279.

Xu, W., Zhang, H., Luo, B., Guo, L., Yang, H., 2015. Adakite-like geochemical signature produced by amphibole-dominated fractionation of arc magmas: An example from the Late Cretaceous magmatism in Gangdese belt, south Tibet. Lithos 232, 197-210.

X. Q., Zeng, L. Z. L., Gao, J. G. J., Zhao, L. Z. L., Wang, Y. W. Y., Hu, Z. H. Z., 2019. Geochemical characteristics and genesis of the Songka Late Cretaceous adakitic high-Mg diorite in the southern margin of Gangdese, southern Tibet. Acta. Petrol. Sin.35, 455-471 (in Chinese with English abstract).

Yang, J., Wu, F., Chung, S., Wilde, S. A., Chu, M., 2006. A hybrid origin for the Qianshan A-type granite, northeast China: Geochemical and Sr–Nd–Hf isotopic evidence. Lithos 89, 89-106.

Yang, H., Ge, W., Zhao, G., Dong, Y., Xu, W., Ji, Z., Yu, J., 2015a. Late Triassic intrusive complex in the Jidong region, Jiamusi–Khanka Block, NE China: Geochemistry, zircon U–Pb ages, Lu–Hf isotopes, and implications for magma mingling and mixing. Lithos 224, 143-159.

Yang, Z., Lu, Y., Hou, Z., Zhang, Z., 2015b. High-Mg Diorite from Qulong in Southern Tibet: Implications for the Genesis of Adakite-like Intrusions and Associated Porphyry Cu Deposits in Collisional Orogens. J. Petrol. 56, 227-254.

Ye, L., Zhao, Z., Liu, D., Zhu, D., Dong, G., Mo, X., Hu, Z., Liu, Y., 2015. Late Cretaceous diabase and granite dike in Namling, Tibet: Petrogenesis and implications for extension. Acta. Petrol. Sin. 31, 1298-1312 (in Chinese with English abstract).

Yin, A., Harrison, T. M., 2000. Geologic evolution of the Himalayan-Tibetan orogen. Annu. Rev. Earth Pl. Sc. 28, 211-280.

Yin, J.Y., Chen, W., Xiao, W.J., Yuan, C., Windley, B.F., Yu, S., Cai, K.D., 2017.Late Silurian–early Devonian adakitic granodiorite, A-type and I-type granites in NW

Junggar, NW China: partial melting of mafic lower crust and implications for slab roll-back. Gondwana Res. 43, 55–73

Yin, C., Ou, J., Long, X., Huang, F., He, X., 2019. Late Cretaceous Neo-Tethyan slab roll-back: Evidence from zircon U-Pb-O and whole-rock geochemical and Sr-Nd-Fe isotopic data of adakitic plutons in the Himalaya-Tibetan Plateau. Geol. Soc. Am. Bull. 326, 144-157.

Zhang, H., Gao, S., Zhong, Z., Zhang, B., Zhang, L., Hu, S., 2002. Geochemical and Sr–Nd–Pb isotopic compositions of Cretaceous granitoids: constraints on tectonic framework and crustal structure of the Dabieshan ultrahigh-pressure metamorphic belt, China. Chem. Geol. 186, 281-299.

Zhang, L., Ducea, M., Ding, L., Pullen, A., Kapp, P., Hoffman, D., 2014. Southern Tibetan Oligocene-Miocene adakites: A record of Indian slab tearing. Lithos 210-211, 209-223.

Zhang, L., Guo, Z., Zhang, M., Cheng, Z., Sun, Y., 2017. Post-collisional potassic magmatism in the eastern Lhasa terrane, south Tibet: Products of partial melting of mélanges in a continental subduction channel. Gondwana Res. 41, 9-28.

Zhang, L., Zhu, D., Wang, Q., Zhao, Z., Liu, D., Xie, J., 2019. Late Cretaceous volcanic rocks in the Sangri area, southern Lhasa Terrane, Tibet: Evidence for oceanic ridge subduction. Lithos, 144-157.

Zhang, Z., Zhao, G., Santosh, M., Wang, J., Dong, X., Shen, K., 2010. Late Cretaceous charnockite with adakitic affinities from the Gangdese batholith, southeastern Tibet: Evidence for Neo-Tethyan mid-ocean ridge subduction? Gondwana Res. 17,

615-631.

Zhang, Z., Ding, H., Palin, R. M., Dong, X., Tian, Z., Chen, Y., 2020. The lower crust of the Gangdese magmatic arc, southern Tibet, implication for the growth of continental crust. Chem. Geol. 77, 136-146.

Zhao, Z., Mo, X., Dilek, Y., Niu, Y., Depaolo, D. J., Robinson, P., Zhu, D., Sun, C., Dong, G., Zhou, S., 2009. Geochemical and Sr-Nd-Pb-O isotopic compositions of the post-collisional ultrapotassic magmatism in SW Tibet: Petrogenesis and implications for India intra-continental subduction beneath southern Tibet. Lithos 113, 190-212.

Zheng, Y., Hou, Z., Gong, Y., Liang, W., Sun, Q., Zhang, S., Fu, Q., Huang, K., Li, Q., Li, W., 2014. Petrogenesis of Cretaceous adakite-like intrusions of the Gangdese Plutonic Belt, southern Tibet: Implications for mid-ocean ridge subduction and crustal growth. Lithos 190-191, 240-263.

Zhu, D., Zhao, Z., Pan, G., Lee, H., Kang, Z., Liao, Z., Wang, L., Li, G., Dong, G., Liu, B., 2009. Early cretaceous subduction-related adakite-like rocks of the Gangdese Belt, southern Tibet: Products of slab melting and subsequent melt–peridotite interaction? J. Asian Earth Sci. 34, 298-309.

Zhu, D., Zhao, Z., Niu, Y., Mo, X., Chung, S., Hou, Z., Wang, L., Wu, F., 2011. The Lhasa Terrane: record of a microcontinent and its histories of drift and growth. Earth Planet. Sci. Lett. 301, 241-255.

Zhu, D., Zhao, Z., Niu, Y., Dilek, Y., Hou, Z., Mo, X., 2013. The origin and pre-Cenozoic evolution of the Tibetan Plateau. Gondwana Res. 23, 1429-1454.

Zhu, D., Wang, Q., Zhao, Z., 2017.Constraining quantitatively the timing and process of continent-continent collision using magmatic record: Method and examples. Sci. China Earth. Sci,60, 1040-1056.

## Figure Captions

**Figure 1**. Maps of the research area. (a) Lhasa terrane in the context of the Tibetan Plateau after Zhu et al. (2011). (b) Tectonic subdivision of Lhasa terrane, southern Tibetan Plateau with study area, after Zhu et al. (2011). (c) Distribution of the Gangdese Batholith outcrop area in the Lhasa terrane, modified from Ma et al. (2013). Locations of dated late Cretaceous (~100–80 Ma) adakitic rocks are indicated; Data sources: U-Pb ages of late Cretaceous adakitic rocks in southern terrane (Wen et al., 2008; Zhang et al., 2010, 2019; Jiang et al., 2012; Ma et al., 2013; Zheng et al., 2014; Chen et al., 2015a, 2015b; Xu et al., 2015; Meng et al., 2019; Yin et al., 2019; Huang et al., 2020). (d) Simplified geological map of the Zeyu-Cuojielin are near Chanang; sample locations are marked. Abbreviations: BNS = Bangong–Nujiang suture zone; IYS = Indus–Yarlung Zangbo Suture Zone; SL = Southern Lhasa terrane, CL = Central Lhasa terrane; and NL = Northern Lhasa terrane.

**Figure 2**. Field and petrographic photos. (a) Field photograph of Zeyu granite SK1307 with K-feldspar phenocrysts and dark microgranular mafic enclave (MME). (b) Hand-sample photograph of Cuojielin quartz syenite SK1315. (c) Needle-like apatite in Zeyu MME (SK1302) (Plane-polarized light). (d) Photomicrograph of Zeyu granite SK1307 (crossed polars). (e) Photomicrograph of Cuojielinquartz syenite SK1313 (crossed polars). (f) Photomicrograph of Cuojielin quartz syenite SK1314 (crossed polars). Abbreviations: Q = quartz; Pl = plagioclase; Kfs = K-feldspar; Mc = microcline; Amp = amphibole; Bt = biotite; Ttn = titanite; Ap = apatite; Mt = magnetite.

**Figure 3.** Representative CL images and U-Pb zircon concordia diagrams. Small red

circles show the locations of LA-ICP-MS U-Pb analysis spots. Large white dashed circles show the locations of corresponding Lu-Hf isotope analyses.

**Figure 4.** Whole-rock geochemistry diagrams. (a) $Na_2O$ + $K_2O$ versus $SiO_2$, after Middlemost (1994). (b) A/CNK vs. A/NK [ A/CNK = molar $Al_2O_3$ / ($CaO+K_2O+Na_2O$); A/NK = molar $Al_2O_3/(K_2O+Na_2O)$] diagram, after Maniar and Piccoli (1989). (c) $K_2O$ vs. $SiO_2$, after Peccerillo (1992). (d) MgO vs. $SiO_2$ diagram; thickened lower crust-derived adakites after Petford and Atherton (1996); subducted oceanic slab-derived adakites after Stern and Kilian (1996) and references therein. (e) $TiO_2$vs. $SiO_2$ diagram. (f) $P_2O_5$ vs. $SiO_2$ diagram. Data sources: late Cretaceous adakitic rocks in southern Lhasa terrane (Zheng et al., 2014; Chen et al., 2015a, 2015b; Dai et al., 2018; Wu et al., 2018; Liu et al., 2019; Meng et al., 2019; Tang et al., 2019; Huang et al., 2020; Shi et al., 2020); Miocene adakitic rocks in southern Lhasa terrane (Hou et al., 2004; Li et al., 2011, 2017; Hu et al., 2017; Sun et al.,2018).

**Figure 5.** Trace element results. (a) Chondrite-normalized rare earth element patterns of Zeyu samples; (b) primitive mantle-normalized trace element patterns of Zeyu samples; (c) REE patterns of Cuojielin samples; (d) primitive mantle-normalized patterns of Cuojielin samples. Chondrite normalization from Boynton (1984); primitive mantle normaliztion from Sun and McDonough (1989).

**Figure 6.** Isotopic data. (a) Sr and Nd isotopic compositions of the Zeyu-Cuojielin intrusive rocks in southern Tibet, modified from Wu et al. (2018) and Wang et al. (2020a). (b) Percentage contribution of mantle material, calculated by zircon Hf isotopes, to late Cretaceous adakite-like magmatic rocks, plotted against zircon ages,

modified from Zhu et al. (2011). Data sources are same as in Fig. 4.

**Figure 7.** Zircon trace elements. (a) Chondrite-normalized rare earth element patterns of zircons in Zeyu host rocks. (b) Chondrite-normalized rare earth element patterns of zircons in Cuojielin quartz syenite. (c) Trace element correlations for zircons from different rock types, after Belousova et al. (2002). (d) Ti-in-Zircon temperature vs. Ce(IV)/Ce(III) of Zeyu host rocks and Cuojielin quartz syenite.

**Figure 8.** Discrimination diagrams for adakite and A-type granites. (a) Sr/Y vs Y, after Defant and Drummond (1990); (b) $(La/Yb)_N$ vs. $Yb_N$ after Petford and Atherton (1996) and Liu et al. (2017) . (c) $Na_2O+ K_2O$ vs. 10000Ga/Al, after Whalen et al. (1987). (d) $(Na_2O+ K_2O)/CaO$ vs. Zr+Nb+Ce+Y, after Whalen et al. (1987). (e) $K_2O+Na_2O$-CaO vs. $SiO_2$. (f) FeO*/(FeO*+MgO) vs. $SiO_2$, modified from Frost et al. (2001) and Frost and Frost (2011). Data sources are same as in Fig. 4.

**Figure 9.** Petrogenetic diagrams. (a) Ba vs. Nb/Y. (b) Sr/Nd vs. Th/Yb.

**Figure 10.** Diagrams that address influence of residual or fractionated minerals. (a) $(^{87}Sr/^{86}Sr)_i$ vs $SiO_2$; (b) $(Dy/Yb)_N$ vs $(La/Sm)_N$. (c) La/Sm vs Sm/Yb, modified from Kay and Mpodozis (2001); (d) La/Yb vs La; (e) Eu/Eu* vs $SiO_2$; (f) $CaO/Na_2O$ vs $Al_2O_3/TiO_2$, modified from Sylvester, (1998). Data sources are same as in Fig. 4.

**Figure 11.** Trace element modelling. (a) Eu/Eu* vs. Rb/Sr. (b) modelling of REEs (30-60% fractionation of MMEs). Partition coefficients from https://earthref.org/KDD/.

**Figure 12.** Temporal and spatial distribution of late Cretaceous magmatic rocks (100-80 Ma) in the southern Lhasa terrane. (a) Histogram of $SiO_2$ contents. (b) $SiO_2$ contents and $\varepsilon_{Nd}(t)$ vs. ages. (c) Latitudes vs. ages. Data of late Cretaceous magmatic rocks in southern Lhasa terrane are from Wen et al. (2008, 2008a), Zhang et al. (2010, 2014, 2019), Chu et al. (2011), Tafti et al. (2011), Zhu et al. (2011), Jiang et al. (2012, 2014, 2015), Ma et al. (2013, 2013a, 2013b, 2015), Ji et al. (2014), Zheng et al. (2014), Chen et al. (2015a, 2015b), Xu et al. (2015, 2019), Ye et al. (2015), Gao et al. (2017), Dai et al. (2018), Wu et al. (2018), Liu et al. (2019), Meng et al. (2019, 2020), Tang et al. (2019), Yin et al. (2019), Huang et al. (2020).

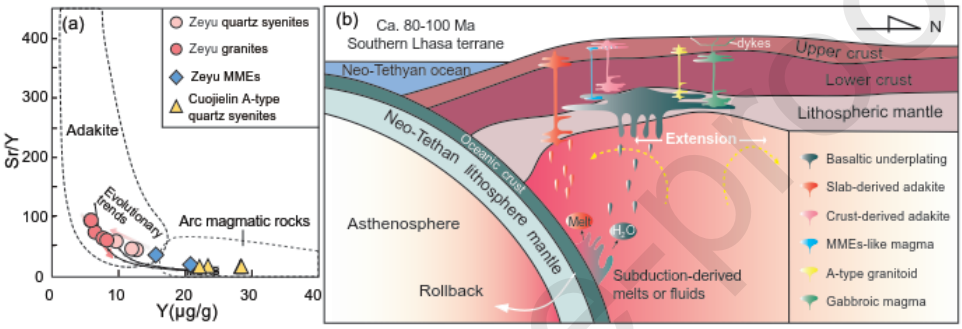


- Adakitic signature originated from residual or fractionated amphibole
- Coeval A-type quartz syenites were produced from fractional

crystallization

- Neo-Tethyan subduction system underwent rollback during late Cretaceous.

**Zhenzhen Wang**: Writing - Original Draft, Conceptualization, Methodology. **Zhidan Zhao**: Writing- Reviewing and Editing, Supervision. **Xuping Li**: Supervision. **Dong Liu**: Supervision. **Xuanxue Mo**: Resources. **Paul D. Asimow**: Writing- Reviewing and Editing, Supervision. **Ningyuan Qi**: Data Curation. **Yan Tang**: Data Curation. **Qing Wang**: Methodology. **Di-Cheng Zhu**: Methodology. **Liangliang Zhang**: Methodology. **Lawangin Sheikh**: Data curation.

Wang et al. Fig.1 W190mm-H127mm (2-column fitting image)

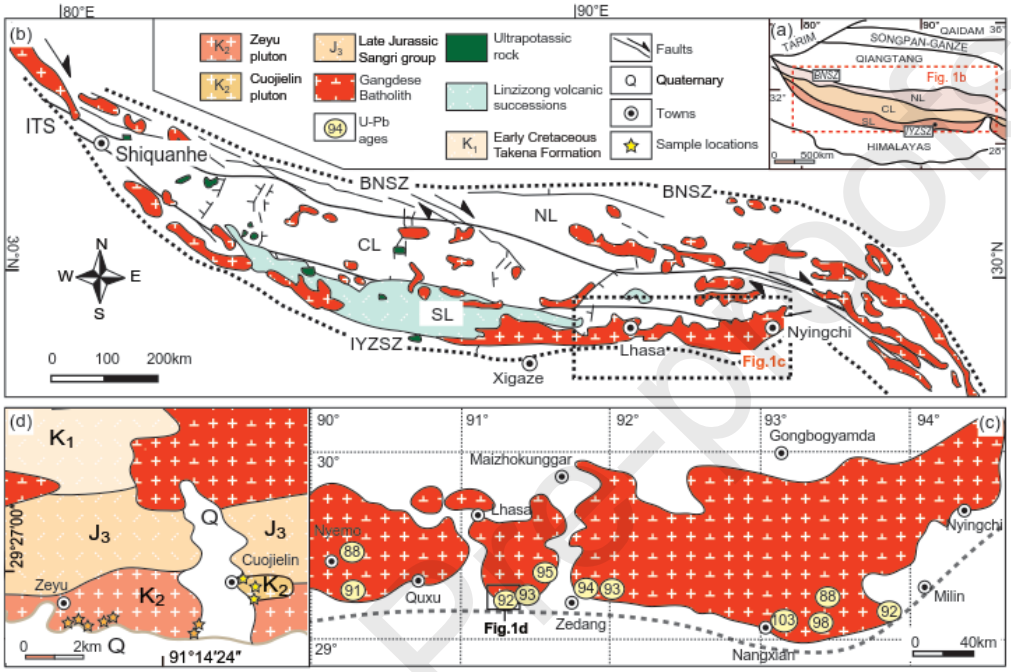

Wang et al. Fig.2 W141mm-H147mm (2-column fitting image)

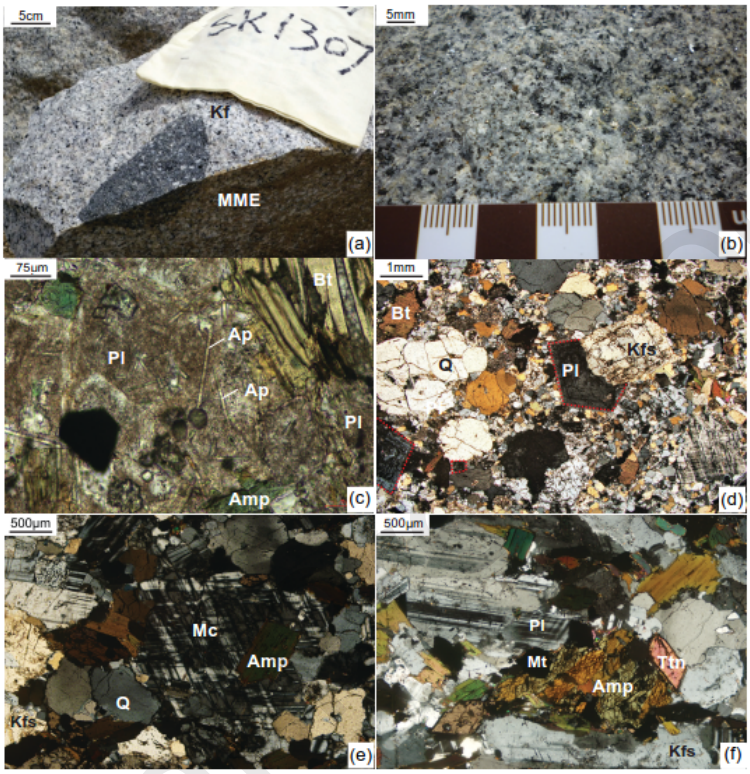

Wang et al. Fig.3 W149mm-H122 mm (2-column fitting image)

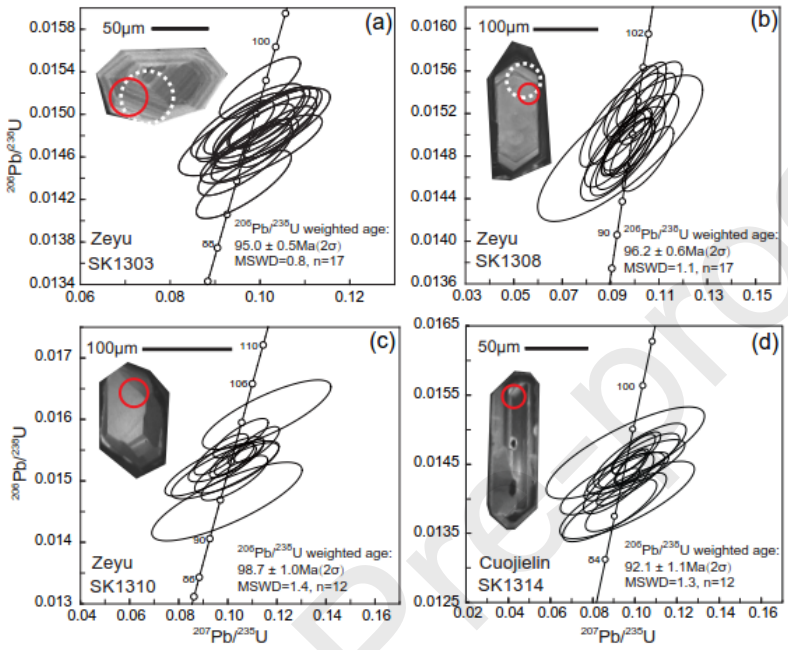

Wang et al. Fig.4 W166mm-H191mm (2-column fitting image)

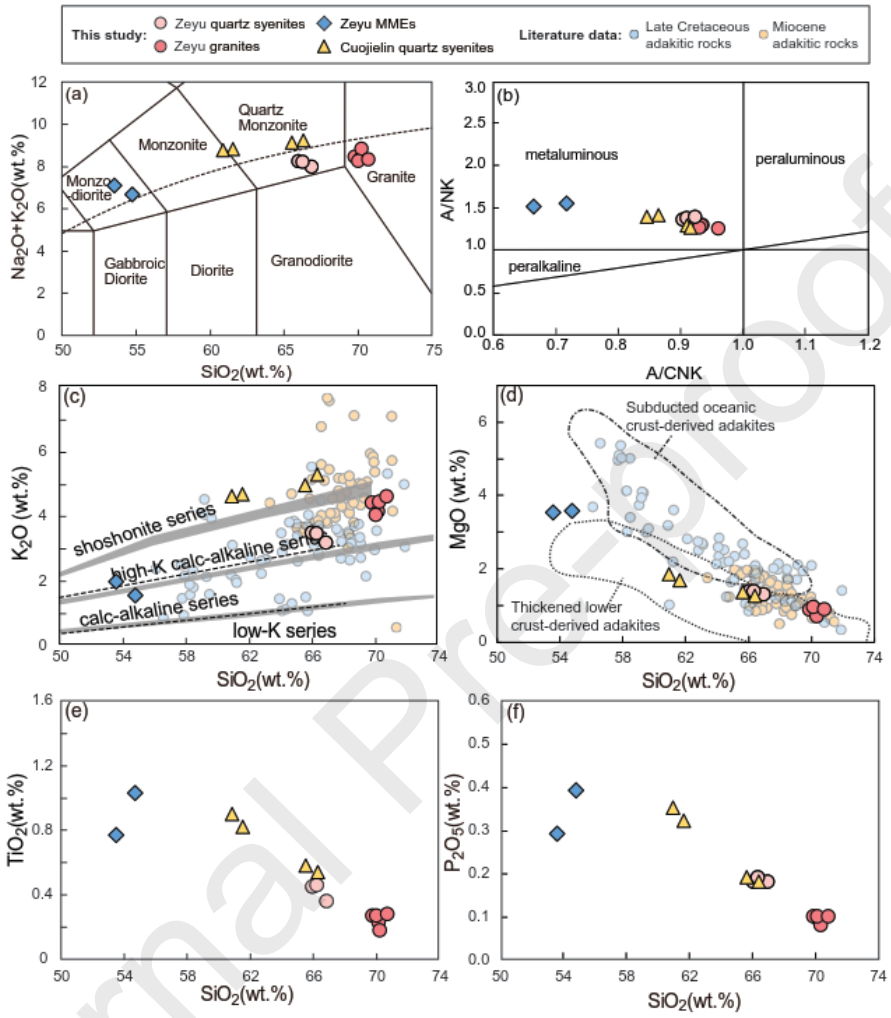

Wang et al. Fig.5 W163mm-H113mm (2-column fitting image)

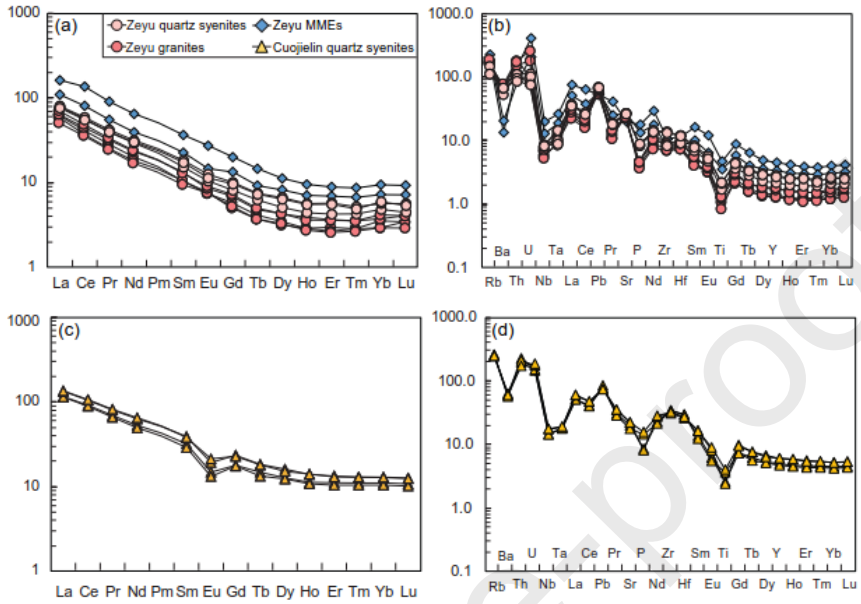

Wang et al. Fig.6 W160mm-H071mm (2-column fitting image)

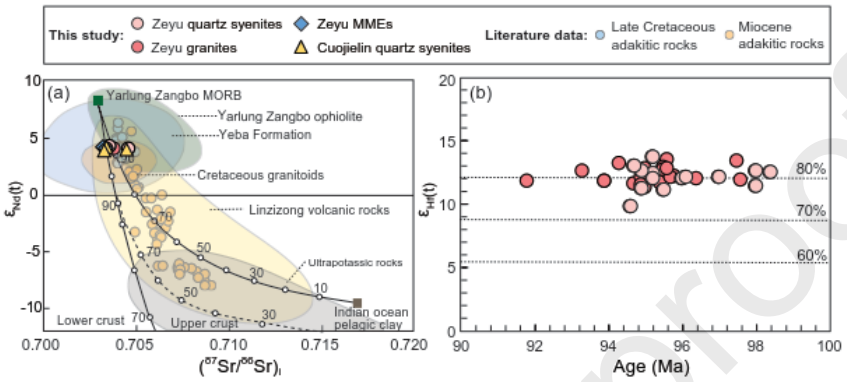

Wang et al. Fig.7 W170mm-H117mm (2-column fitting image)

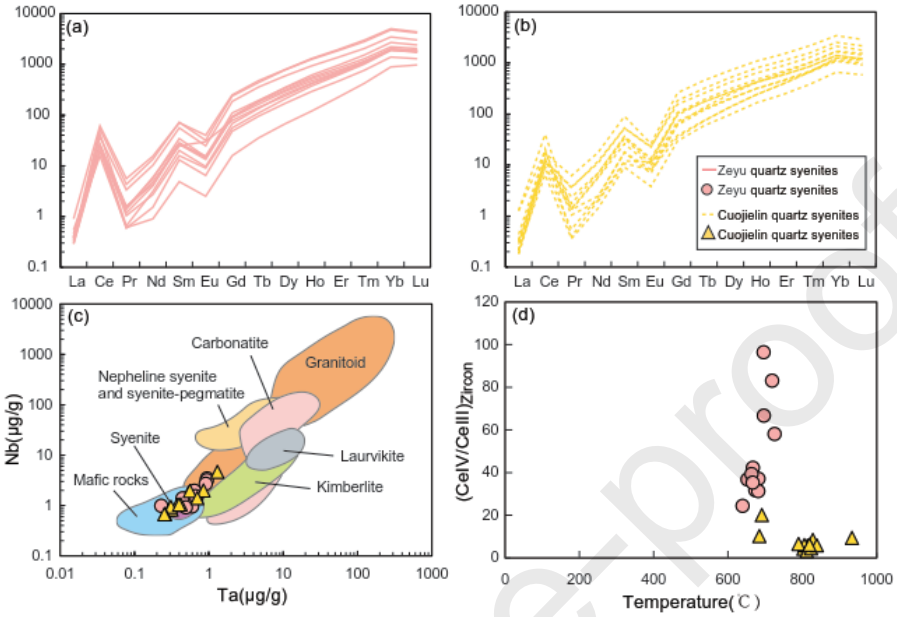

Wang et al. Fig.8 W170mm-H190mm (2-column fitting image)

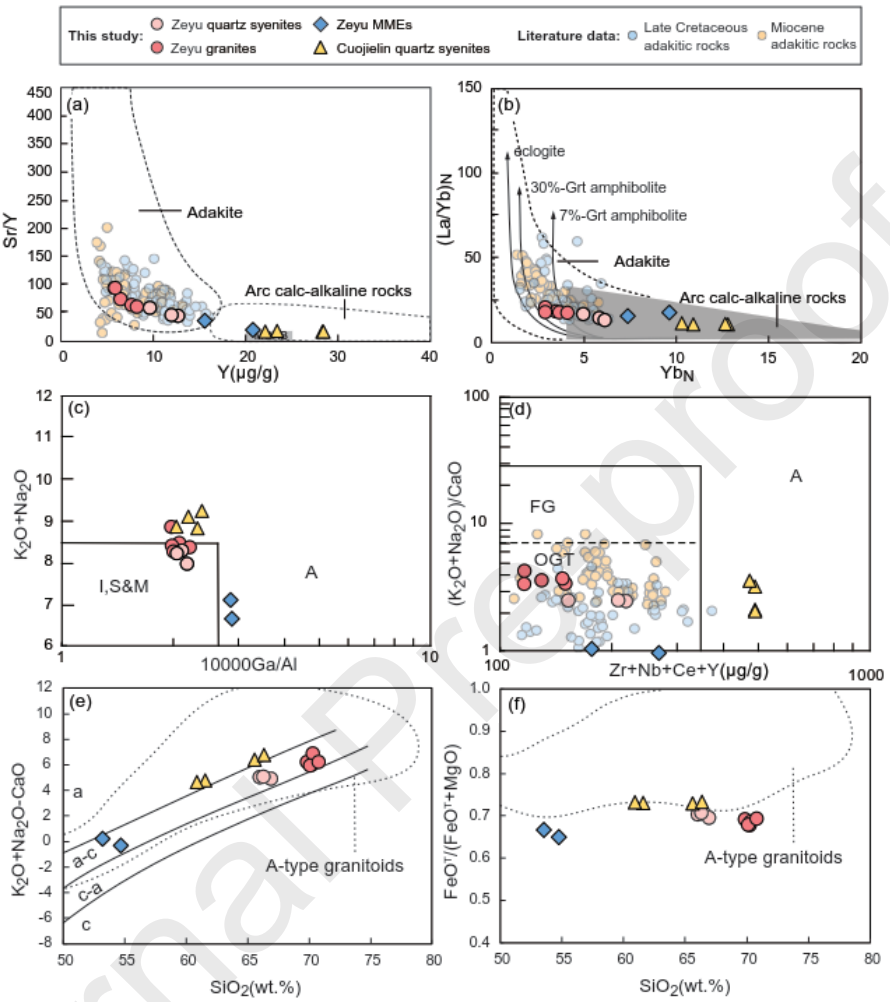

Wang et al. Fig.9 W170mm-H060mm (2-column fitting image)

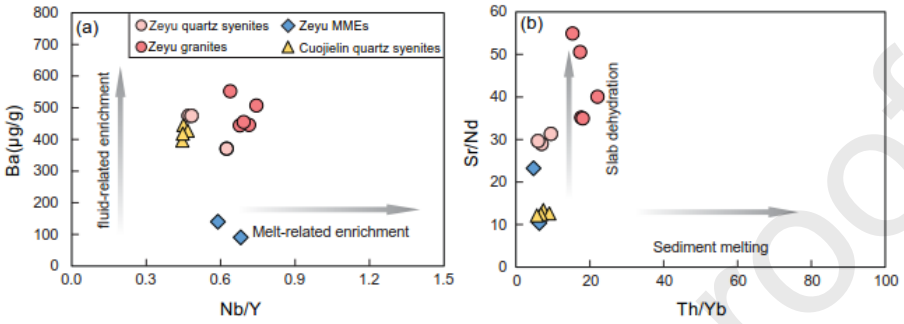

Wang et al. Fig.10 W174mm-H196mm (2-column fitting image)

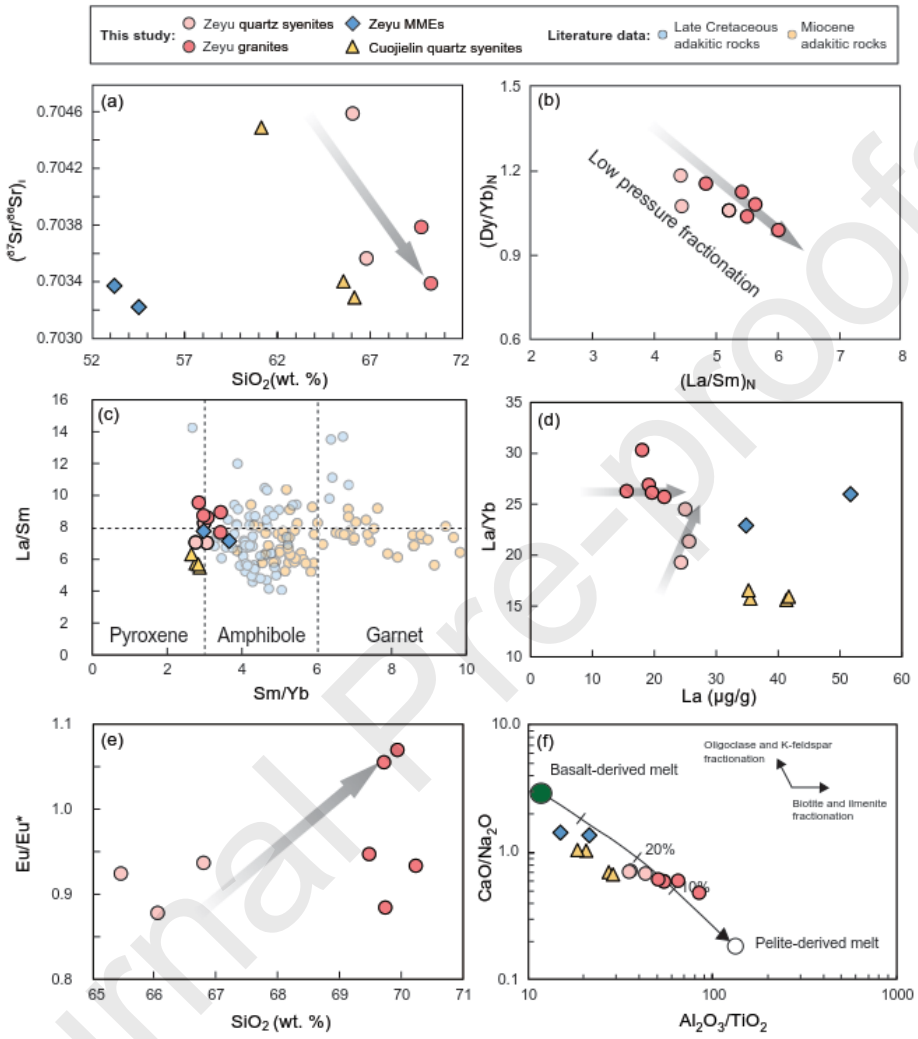

Wang et al. Fig.11 W162mm-H058mm (2-column fitting image)

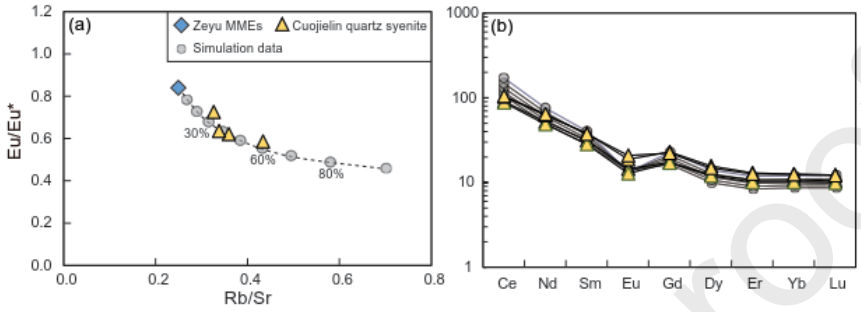

Wang et al. Fig.12 W095mm-H183mm (1-column fitting image)

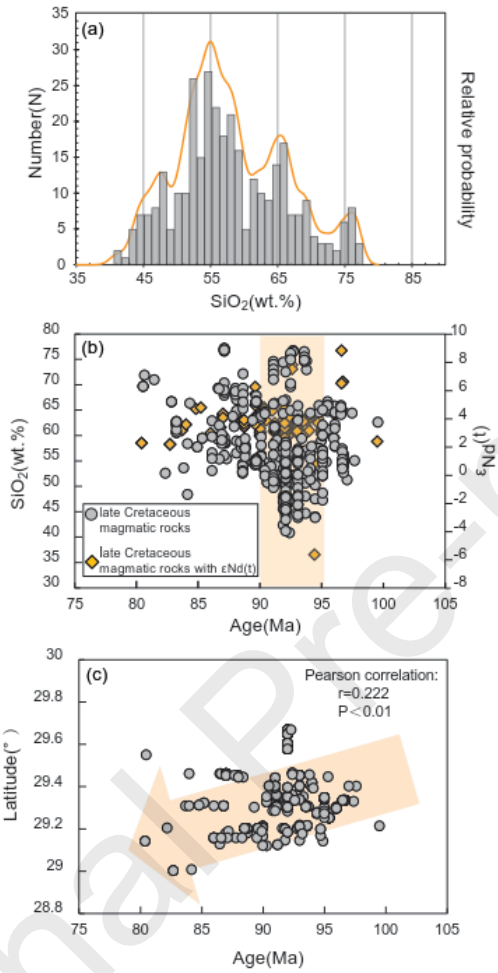




**Declaration of interests**

☒ The authors declare that they have no known competing financial interests or personal relationships that could have appeared to influence the work reported in this paper.

☐The authors declare the following financial interests/personal relationships which may be considered as potential competing interests: